The Astrophysical Journal, 618:259–280, 2005 January 1

SPATIALLY RESOLVED CHEMISTRY IN NEARBY GALAXIES. I. THE CENTER OF IC 342

David S. Meier
Department of Astronomy, University of Illinois, 1002 West Green Street, Urbana, IL 61801; meierd@astro.uiuc.edu

and

Jean L. Turner[1]
Department of Physics and Astronomy, UCLA, Los Angeles, CA 90095-1547; turner@astro.ucla.edu
Received 2004 July 29; accepted 2004 October 1

ABSTRACT

We have imaged emission from the millimeter lines of eight molecules—C_2H, $C^{34}S$, N_2H^+, CH_3OH, HNCO, HNC, HC_3N, and SO—in the central half-kiloparsec of the nearby spiral galaxy IC 342. The 5″ (∼50 pc) resolution images were made with the Owens Valley Millimeter Array. Using these and previously published CO and HCN images, we obtain a picture of the chemistry within the nuclear region on the size scales of individual giant molecular clouds. Bright emission is detected from all but SO. There are marked differences in morphology for the different molecules. A principal-component analysis is performed to quantify similarities and differences among the images. This analysis reveals that while all molecules are to zeroth order correlated, that is, that they are all found in dense molecular clouds, there are three distinct groups of molecules distinguished by the location of their emission within the nuclear region. N_2H^+, $C^{18}O$, HNC, and HCN are widespread and bright, good overall tracers of dense molecular gas. C_2H and $C^{34}S$, tracers of photodissociation region chemistry, originate exclusively from the central 50–100 pc region, where radiation fields are high. The third group of molecules, CH_3OH and HNCO, correlates well with the expected locations of bar-induced orbital shocks. The good correlation of HNCO with the established shock tracer molecule CH_3OH is evidence that this molecule, whose chemistry has been uncertain, is indeed produced by the processing of grain mantles. HC_3N is observed to correlate tightly with 3 mm continuum emission, demonstrating that the young starbursts are the sites of the warmest and densest molecular gas. We compare our HNC images with the HCN images of Downes and coworkers to produce the first high-resolution, extragalactic HCN/HNC map: the HNC/HCN ratio is near unity across the nucleus, and the correlation of both of these gas tracers with star formation is excellent. The ratio exhibits no obvious correlation with gas temperature or star formation strength.

Subject headings: astrochemistry — galaxies: individual (IC 342) — galaxies: ISM — galaxies: starburst — radio lines: galaxies

1. INTRODUCTION

The bright and abundant molecule CO has dominated the study of molecular clouds in external galaxies. The millimeter-wave transitions of CO and its isotopomers are powerful probes of diffuse molecular gas (e.g., Young & Scoville 1991). However, emission from the optically thick and easily excited CO tends to favor the warmer, radiatively lit, and diffuse surface layers of clouds (e.g., Turner et al. 1993; Meier et al. 2000, hereafter MTH00). Since dense gas is the component most closely connected to star formation (e.g., Gao & Solomon 2004), to understand the links between molecular clouds and star formation in different galactic environments, we need to study tracer molecules appropriate to a cooler, dense component that may not be well traced by CO.

Each molecular line traces a distinct regime of density and temperature within a molecular cloud, while different molecules can trace different gas chemistries (see van Dishoeck & Blake 1998 for a review of Galactic astrochemistry). Emission from high-density tracers such as HCN, HCO^+, and CS shows that large amounts of dense ($\gtrsim 10^4$ cm^{-3}) molecular gas are present in the centers of galaxies (e.g., Mauersberger & Henkel 1989; Mauersberger et al. 1989; Nguyen-Q-Rieu et al. 1989, 1992; Solomon et al. 1992; Helfer & Blitz 1993) and that the dense molecular interstellar medium (ISM) can vary significantly on scales of a few tens of parsecs (e.g., Downes et al. 1992; Brouillet & Schilke 1993; Helfer & Blitz 1997; Seaquist et al. 1997; Sorai et al. 2002).

Numerous molecules have been detected in nearby starbursts (e.g., Henkel et al. 1987, 1988; Nguyen-Q-Rieu et al. 1991; Mauersberger et al. 1991, 1995; Petuchowski & Bennett 1992; Sage & Ziurys 1995; Martín et al. 2003; Usero et al. 2004; Wang et al. 2004). These studies find that the chemical differentiation seen within Galactic molecular clouds survives to scales of hundreds of parsecs, and even to galaxy-wide differences. However, most of these observations have been done with single-dish telescopes at resolutions of ∼30″, or a few hundred pc on the galaxy, and thus average many giant molecular clouds (GMCs) together into one beam.

With millimeter interferometers it is now possible to resolve individual GMCs in the nearest galaxies with sufficient sensitivity to allow the study of selected chemical species (e.g., García-Burillo et al. 2000, 2001, 2002). Because of the low (∼50–100 pc) physical resolution, extragalactic observations are insensitive to small-scale (∼tenths of pc) chemistry typically studied in the Galaxy, but such maps can resolve the chemical properties operating over the bulk of a GMC and between individual GMCs. These observations can provide insights regarding the extent to which distinct large-scale properties, such as starbursts, shocks, bars, spiral arms, tidal forces, and AGNs, influence the chemistry of molecular clouds and how these

[1] Visiting Associate, Department of Astronomy, California Institute of Technology, Pasadena, CA 91125.

TABLE 1
Observational Data

Transition	Dates (MMYY)	Frequency (GHz)	T_{sys} (K)	ΔV_{chan} (km s^{-1})	$\Delta\nu_{band}$ (MHz)	Beam (arcsec, deg)	Noise (mK/mJy beam^{-1})
C_2H (1–0, 3/2–1/2)[a]	0900–1000	87.317	350–690	13.73	128	5.5 × 4.9, −41	53/8.9
HNCO (4_{04}–3_{03})[a]	0900–1000	87.925	420–780	13.64	128	5.9 × 5.1, −36	39/7.4
HNC (1–0)[a]	0900–1000	90.664	430–930	13.23	128	5.9 × 5.1, −39	26/5.2
HC_3N (10–9)[a]	0900–1000	90.979	400–890	13.18	128	5.9 × 5.1, −44	24/4.8
N_2H^+ (1–0)[a]	0101–0401	93.174	380–440	12.87	128	6.2 × 5.1, −59	29/6.4
$C^{34}S$ (2–1)[a]	0101–0401	96.413	370–450	12.44	128	6.6 × 5.6, −63	24/6.8
CH_3OH (2_k–1_k)[a]	0101–0401	96.741	420–480	12.40	240	6.0 × 4.8, −65	35/7.6
SO (2_3–1_2)[b]	1097–1297	109.252	410–480	10.98	128	5.0 × 4.3, −21[c]	41/8.6
SO (6_5–5_4)[b]	1097–1297	219.949	410–1020	5.45	128	5.0 × 4.3, −21[d]	52/44

[a] Phase center 1: $\alpha = 3^h41^m57^s.0$, $\delta = +67°56'30''.0$ (B1950.0); $v_{LSR} = 35$ km s^{-1}.
[b] Phase center 1: $\alpha = 3^h41^m57^s.0$, $\delta = +67°56'26''.0$ (B1950.0); $v_{LSR} = 35$ km s^{-1}. Phase center 2: $\alpha = 3^h41^m57^s.9$, $\delta = +67°56'29''.0$ (B1950.0); $v_{LSR} = 35$ km s^{-1}.
[c] Maps generated with a 50 kλ taper.
[d] Map convolved to the same resolution as the 3 mm SO transition.

influences are transmitted from the GMC scale to the galaxy as a whole.

We have surveyed the nearby Scd galaxy IC 342 in transitions from eight astrochemically important molecules. C_2H, HNCO, HNC, HC_3N, N_2H^+, $C^{34}S$, CH_3OH, and SO were imaged at ∼50 pc resolution with the Owens Valley Millimeter Array (OVRO). These are the first published interferometer maps of these lines in an external galaxy. IC 342 is the nearest ($D \sim 2$ Mpc)[2] gas-rich spiral with active star formation in its nucleus (Becklin et al. 1980; Turner & Ho 1983), and the first galaxy to be mapped with millimeter interferometers (Lo et al. 1984). There is widespread resolvable molecular gas distributed in both dense clouds, with masses similar to Sgr B2, and a diffuse medium about the size of the central molecular zone (Morris & Serabyn 1996) in the Milky Way. Detailed knowledge of the H_2 column densities, excitation temperatures, and densities in IC 342 exists from CO and its isotopomers as a basis for comparison with these new lines (Ishizuki et al. 1990; Downes et al. 1992; Turner & Hurt 1992; Wright et al. 1993; Turner et al. 1993; MTH00; Meier & Turner 2001, hereafter MT01).

[2] Because of its location behind the Galactic plane, IC 342's distance is still a matter of debate. Recent studies have argued for a distance of ∼3 Mpc (e.g., Saha et al. 2002; Karachentsev et al. 2003), but we adopt the shorter distance to maintain consistency with our previous work.

2. OBSERVATIONS

We observed eight lines at 3 mm and one line at 1 mm with OVRO between 1997 October 22 and 2001 April 7 (Table 1). The interferometer consisted of six 10.4 m antennas with SIS receivers (Padin et al. 1991; Scoville et al. 1994). All transitions were observed in the C and L array configurations except for the SO, which was observed in L and H.

Table 1 lists the observed lines along with the observational parameters. The transitions were selected based on the criteria that (1) they are bright in Sgr B2 ($T_a \gtrsim 1$ K in the Turner 1989 spectral line survey), (2) they sample a selection of different types of chemistry, and (3) they maximize the number of species OVRO can observe simultaneously. Table 2 lists molecular parameters for the transitions. The nine spectral lines were observed in three sets of spectrometer configurations. C_2H, HNCO, HNC, and HC_3N were observed as a group, as were CH_3OH, $C^{34}S$, and N_2H^+, and the two SO transitions were observed with $C^{18}O$ (MT01). Each group has the same instrumental

TABLE 2
Molecule and Column Density Parameters

Molecular Transition	μ (D)	A/B/C (GHz)	$S_{ul}g_Kg_I$	E_u (K)	$^{H_2}n_{cr}/^{e}n_{cr}$[a] log(cm^{-3})	$N(50)/N(10)$[b]	T_{min}[c] (K)	N_{min}/N_{10}[d]
C_2H (1–0, 3/2–1/2)	0.8	.../43.675/...	1	4.19	5.13/6.06	3.01	4.80	0.66
HNCO (4_{04}–3_{03})	1.60	912.711/11.071/10.911	4	10.55	5.43/6.03	4.81	7.03	0.92
HNC (1–0)	3.05	.../45.332/...	1	4.35	6.39/5.69	2.94	4.98	0.70
HC_3N (10–9)	3.72	.../4.5491/...	10	24.02	5.86/6.69	0.723	24.0	0.59
N_2H^+ (1–0)	3.40	.../46.587/...	1	4.47	5.63/5.67	3.00	5.12	0.75
$C^{34}S$ (2–1)	1.96	.../24.104/...	2	6.94	5.65/5.99	2.56	7.29	0.61
CH_3OH (2_k–1_k)	0.89	127.484/24.680/23.770	4, 3, 4[e]	6.98	4.83/6.21	5.96	4.65	0.65
SO (2_3–1_2)	1.55	.../21.523/...	1.51	21.06	5.27/6.10	0.901	21.4	0.68
SO (6_5–5_4)	1.55	.../21.523/...	5.91	34.99	6.55/7.30	0.296	35.3	0.28

Notes.—Data from the JPL Molecular Spectroscopy Catalog (Pickett et al. 1998) and references therein. Collisional coefficients are HNC, C_2H (HCN; Green & Thaddeus 1974), $C^{34}S$, HC_3N (Green & Chapman 1978), N_2H^+ (Green 1975), CH_3OH (Pottage et al. 2004), HNCO (Green 1986), and SO (Green 1994).
[a] The critical density of the transitions neglecting opacity effects ($^{H_2}n_{cr} \simeq A_{ul}/C_{ul}$) and $^{e}n_{cr}$ based on the formalism of Dickinson et al. (1977), with $[e^-] = [C^+] \simeq 1.5 \times 10^{-5}$.
[b] The ratio by which the derived column densities change when T_{ex} is changed from 10 to 50 K.
[c] The T_{ex} value at which derived (LTE) column densities are at a minimum.
[d] The ratio by which the derived column densities change when the T_{ex} value is changed from 10 K to T_{min}.
[e] $S_{ul}g_Kg_I$ for the three blended 2_1–1_1 E, 2_0–1_0 E, and 2_0–1_0 A^+ transitions (e.g., Turner 1991).

configuration, phase center, and weather. Data were calibrated using the MMA package. Phase calibration was done by observing the point source 0224+671 every 20 minutes. Absolute flux calibration is based on observations of Neptune or Uranus and with 3C 273, 3C 84, 3C 454.3, and 3C 345 as supplementary flux calibrators. Based on the derived fluxes and flux histories of these secondary flux calibrators, we estimate that the absolute fluxes are good to 10%–15% for the 3 mm data and 20%–25% for the 1 mm data (SO). The lines of SO (2_3–1_2) and SO (6_5–5_4) were not detected.

Both robustly weighted maps with resolutions of $\sim 5''$–$6''$ and uniformly weighted maps with $\sim 4''$ resolution were produced. The maps are not primary-beam corrected. Data reduction was done with the NRAO AIPS. In making the integrated intensity maps, emission greater than 1.2 σ was included. Continuum emission has not been subtracted from the maps since the 3 mm continuum peak is below 1 σ.

The (u, v) coverages imply that emission on scales larger than $\sim 50''$ is resolved out. To estimate the amount of extended flux missing from the images, each map was compared with its single-dish spectrum. Although somewhat uncertain due to the low signal-to-noise ratio of some of the single-dish detections (Henkel et al. 1988; Mauersberger & Henkel 1991b; Nguyen-Q-Rieu et al. 1991; Mauersberger et al. 1995; Hüttemeister et al. 1995a, 1997), all species are consistent with no flux being resolved out, except possibly HC_3N. This is consistent with what is found for ^{13}CO and $C^{18}O$ (MTH00; MT01) toward IC 342 and is expected for these dense gas tracers. In the case of HC_3N, the interferometer HC_3N flux is $\sim$30% of the claimed tentative detection by IRAM (Henkel et al. 1988), but given its very high dipole moment it is not expected to be extended on $\sim$50 pc scales. This implies that the claimed single-dish brightness for HC_3N was overestimated, and not that the interferometer resolves out significant flux.

3. IC 342 AND ITS MOLECULES

3.1. *A Sketch of the Nucleus of IC 342*

We have a basic understanding of the small-scale molecular structure of IC 342's nucleus from studies of CO, its isotopomers, and HCN (Ishizuki et al. 1990; Turner & Hurt 1992; MTH00; MT01; Schulz et al. 2001; Mauersberger et al. 2003). A CO (1–0) map of IC 342 (Levine et al. 1994) is shown atop a *Hubble Space Telescope* (*HST*) image of the nucleus in Figure 1. Within the central 300 pc (30″), two molecular arms extend inward (Ishizuki et al. 1990), terminating in a central ring of dense gas (Downes et al. 1992). The total mass of molecular gas within the central kpc is $\sim 4 \times 10^7\ M_\odot$. Orbital timescales here are a few $\times 10^7$ yr. The gas is on pronounced oval orbits, with an estimated radial drift into the nuclear region due to tidal torquing of $\sim 0.1\ M_\odot\ \mathrm{yr}^{-1}$ (Turner & Hurt 1992), which is also the approximate rate of current star formation in the radio/IR source. The central molecular ring surrounds a nuclear star cluster estimated to be 6–60 Myr in age (Böker et al. 1997). The star cluster coincides with a central "trough" of molecular gas, the hole in the molecular ring.

Five prominent GMCs with masses of $\sim 10^6\ M_\odot$ are found within the molecular ring and arms. These clouds have masses slightly less than the Sgr B2 cloud in the Galactic center. GMCs B and C (adopting the nomenclature of Downes et al. 1992) are located where the incoming molecular arms meet the ring. These clouds coincide with two young ($\sim$a few Myr old) large star-forming regions. GMC B is near the more dominant

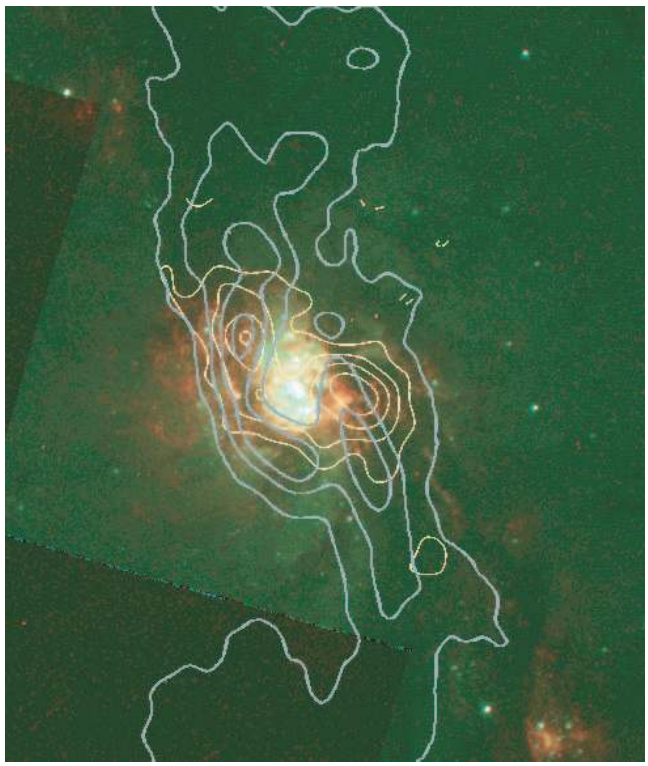

FIG. 1.—Color *HST* composite of IC 342's nucleus. Green/blue shows F555 (*V* band), and red shows Hα+continuum. The blue contours show ^{12}CO (1–0), and the yellow contours show 3 mm (see MT01).

of the two IR/radio star-forming regions, which has a luminosity of $L_{OB} \sim 10^8\ L_\odot$ (Becklin et al. 1980; Turner & Ho 1983), corresponding to an estimated 500 O stars. Cloud C appears somewhat warmer than B in the highest transitions of CO (Harris et al. 1991), but a careful analysis at high resolution in the lower transitions shows that GMC B is actually the warmest location in the nucleus (MT01). GMC A is closest in projection to the nuclear star cluster and dynamical center. GMC A has CO (1–0) and HCN (1–0) properties similar to those of B and C, but much weaker star formation. GMC D, along the northern arm, is also not a site of strong star formation. In this region large gas-streaming motions are observed (Turner & Hurt 1992) along the arms. The resulting shear could slow star formation, although there is some star formation indicated by Hα downstream from the molecular arms.

3.2. *Overview of the Molecules of IC 342*

Figure 2 displays the robustly weighted integrated intensity maps for the seven detected lines plus smoothed maps of previously published ^{12}CO (1–0) and $C^{18}O$ (1–0) (MTH00; MT01). Each map is overlaid on a gray-scale image of ^{12}CO (1–0). Figure 3 displays the higher resolution uniformly weighted maps for the central-ring region overlaid on the gray-scale HCN (1–0) image of Downes et al. (1992). Figures 4 and 5 display spectra for six nuclear clouds. Spectra were generated by summing all the flux within a 6″ box centered on the GMC positions (Table 3). On each spectrum the expected line position of any other lines 0.1 K or brighter based on the spectrum of Sgr B2 (Turner 1989) are indicated. Line intensities are listed in Table 3.

One might naively expect that the molecules would follow the basic CO distribution, since CO is a good overall tracer of

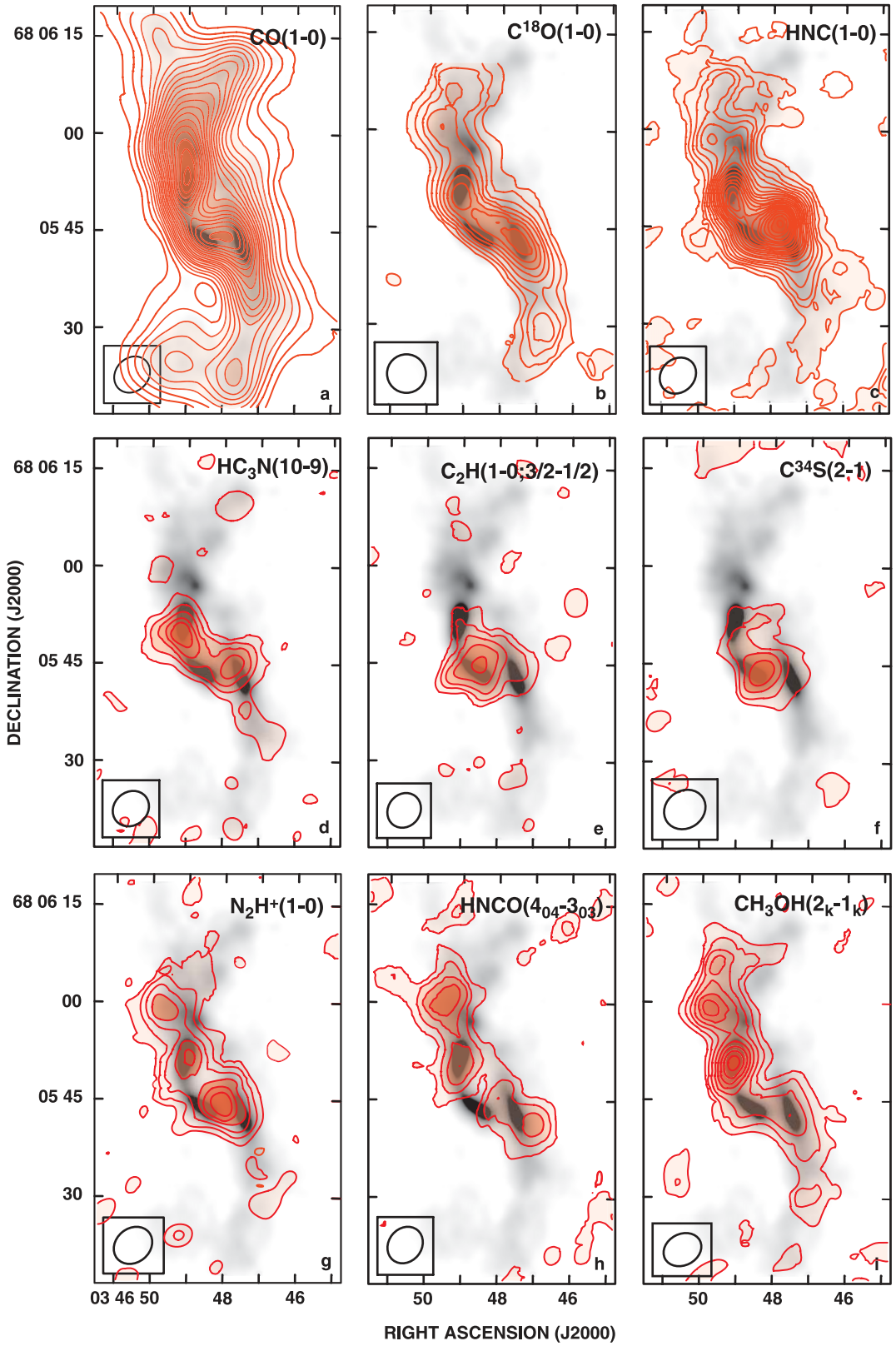

FIG. 2.—Integrated intensities of nine tracer molecules observed toward the nucleus of IC 342. Each map is contoured in steps of 2 times the rms intensity in each map, except for ^{12}CO (1–0). (*a*) ^{12}CO (1–0) transition smoothed to $5'' \times 4''.5$ resolution and contoured in steps of 7.7 K km s^{-1}. (*b*) C^{18}O (1–0) transition contoured in steps of 1.4 K km s^{-1} for $6''.0$ resolution. (*c*) HNC (1–0) transition in steps of 1.5 K km s^{-1}. (*d*) HC_3N (10–9) transition in steps of 1.5 K km s^{-1}. (*e*) C_2H $N(J,F) = 1(3/2,\ 2)-0(1/2,\ 1)$ transition in steps of 3.0 K km s^{-1}. (*f*) C^{34}S (2–1) transition in steps of 1.8 K km s^{-1}. (*g*) N_2H^+ (1–0) transition in steps of 1.6 K km s^{-1}. (*h*) HNCO (4_{04}–3_{03}) transition in steps of 2.1 K km s^{-1}. (*i*) CH_3OH (2_k–1_k) transition in steps of 1.8 K km s^{-1}. The gray scale seen in all frames is of ^{12}CO (1–0) at full resolution ($2''.7 \times 2''.2$; see MTH00) for comparison.

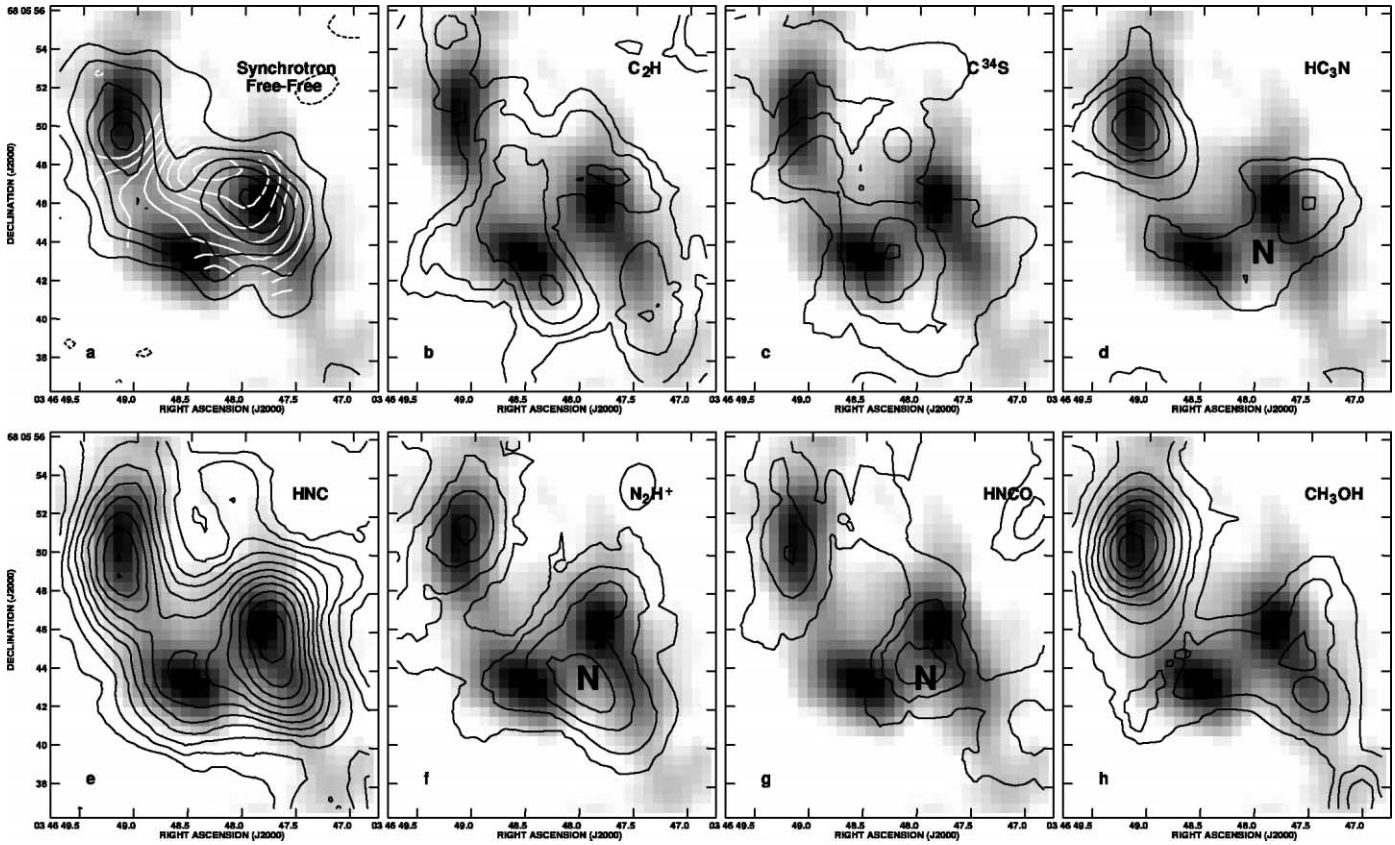

FIG. 3.—Integrated intensities of the seven tracer molecules observed in the central portion of IC 342's nucleus, weighted to optimize spatial resolution at the expense of sensitivity. Each map is contoured at ~2 times the rms noise level in each map except for 6 cm synchrotron. Each transition is overlain by the gray-scale image of HCN (1–0) kindly provided by D. Downes (Downes et al. 1992). The HCN (1–0) gray scale ranges from 10 to 82 K km s^{-1} for a resolution of $2''.8 \times 2''.7$; P.A. $= -180°$. The location of the potential nitrogen core is labeled with "N" in the corresponding panels. (*a*) The 3 mm continuum emission (*black contours*; MT01) in steps of 1 mJy beam^{-1} for a resolution of $3''.3 \times 3''.0$, $-44°.3$, together with the 6 cm synchrotron flux (*white contours*) at the same resolution and contour increment. The 6 cm synchrotron emission is obtained by assuming that the 3 mm continuum emission (MT01) is all thermal free-free and extrapolating this flux to 6 cm, and removing it from the 6 cm continuum flux of Turner & Ho (1983). (*b*) C_2H $N(J, F) = 1(3/2, 2)-0(1/2, 1)$ transition in steps of 3.6 K km s^{-1} for $4''.5 \times 4''.0$, $-21°.7$ resolution. (*c*) $C^{34}S$ (2–1) transition in steps of 3.1 K km s^{-1} for $5''.0 \times 4''.3$, $-51°.7$ resolution. (*d*) HC_3N (10–9) transition in steps of 2.8 K km s^{-1} for $4''.6 \times 4''.1$, $-30°.2$ resolution. (*e*) HNC (1–0) transition in steps of 3.3 K km s^{-1} for $4''.5 \times 4''.0$, $-24°.6$ resolution. (*f*) N_2H^+ (1–0) transition in steps of 2.9 K km s^{-1} for $4''.7 \times 4''.1$, $-37°.3$ resolution. (*g*) HNCO ($4_{04}-3_{03}$) transition in steps of 4.2 K km s^{-1} for $4''.7 \times 4''.0$, $-22°.3$ resolution. (*h*) CH_3OH (2_k-1_k) transition in steps of 2.5 K km s^{-1} for $4''.6 \times 4''.0$, $-51°.7$ resolution.

molecular gas. Or perhaps one might expect to find emission peaks for these molecules preferentially at peaks of HCN peaks, since the molecules of our sample are high-density tracers like HCN. Instead, dramatic variations in morphology are evident among the different transitions. Either the dense gas component of IC 342 has extreme variations in excitation among the GMCs, or there is widespread chemical differentiation across the nucleus. The morphology of the different astrochemical species provides evidence of changing chemical influences due to star formation, physical conditions, and dynamics across the nucleus (§ 5).

Fractional abundances [$X(\mathrm{mol}) \equiv N_{\mathrm{mol}}/N_{\mathrm{H_2}}$] are listed in Table 4, based on molecular parameters in Table 2. Column densities are determined assuming optically thin emission and LTE:

$$N_{\mathrm{mol}} = \left(\frac{3kQe^{E_u/kT_{\mathrm{ex}}}}{8\pi^3 \nu S_{ul} \mu_0^2 g_{K_u} g_{I_u}}\right) I_{\mathrm{mol}}, \qquad (1)$$

where S_{ul}, g, and E_u are the line strength, degeneracy, and upper energy of each state, respectively, and T_{ex} is the excitation temperature associated with the transition. Given that we have mapped only one transition of each species, corrections for background radiation and opacity have been ignored. Column densities are sensitive to T_{ex} through the partition function Q and the energy of the upper state. The asymmetric tops (HNCO and CH_3OH) are more sensitive to temperature changes than the linear rotors. Changes in gas density also affect excitation, particularly for molecules with high critical densities (HNC, N_2H^+, and HC_3N). Fortunately, in IC 342 these properties have been at least partially constrained by observation. The kinetic temperature T_k determined from NH_3 is ~50 K (Ho et al. 1982), which is similar to the derived dust temperature, 42 K (Becklin et al. 1980; Rickard & Harvey 1984). Modeling of the optically thick lines of CO (1–0), CO (2–1), and CO (3–2) indicates temperatures of 15–40 K (Ho et al. 1987; Eckart et al. 1990; Xie et al. 1994); however, the optically thick CO lines may be biased toward the outer, radiation-warmed layers of the clouds (Turner et al. 1993; MT01). We adopt $T_{\mathrm{ex}} = 10$ K determined from $C^{18}O$ interferometer maps (MT01) and single-dish H_2CO and CH_3OH measurements (Hüttemeister et al. 1997) as the most suitable excitation temperature to use with the observed tracer species. Table 2 gives the factor by which the column densities would change if the assumed T_{ex} were changed from 10 to 50 K. Given the critical densities of the

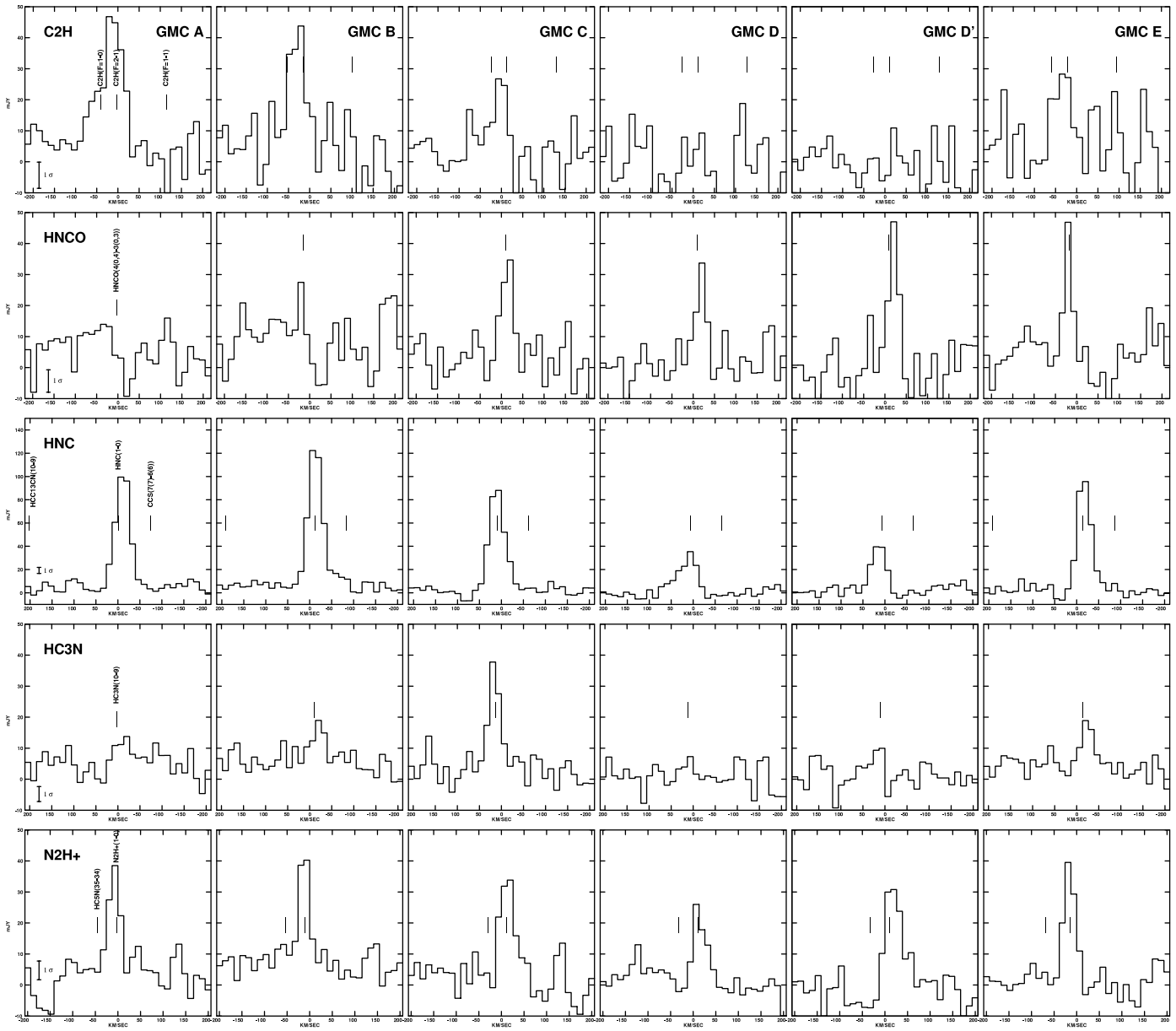

FIG. 4.—Spectra from five of the observed transitions sampled at the locations of the five major GMCs (e.g., Downes et al. 1992). Spectra are summed across a 6″ box centered on the fitted locations of each GMC. Positions for each GMC are taken from high-resolution $C^{18}O$ observations (Table 3 of MT01). GMC A is at the far left of the each set of spectra, extending to GMC E at the far right. Note that the sampled locations do not necessarily align precisely with the peaks of the tracer molecules. In the first plane of each set, any spectral line $T_{mb} \gtrsim 0.1$ K in the Turner (1989) Sgr B2 line survey that falls within the observed bandwidth is labeled. For the remaining four panels these lines are marked by tick marks shifted in velocity to match IC 342's ^{12}CO (1–0) velocity at that location. In all cases the zero velocity corresponds to $v_{LSR} = 35$ km s^{-1} of the transition (the brightest component if there is unresolved hyperfine structure). Also included in the first plane is the 1 σ error bar, determined from the rms in an individual line-free channel.

mapped species, T_{ex} is very likely lower than T_k (subthermal), so 50 K is considered a robust upper limit to the excitation temperature.

Fractional abundances require, in addition, an H_2 column density, $N(H_2)$. $N(H_2)$ is most easily obtained from the CO (1–0) brightness and an empirical Galactic conversion factor X_{CO}. However, X_{CO} overpredicts $N(H_2)$ in nearby galaxy centers, including IC 342, by factors of a few (e.g., MT01; Dahmen et al. 1998; Weiß et al. 2001; Meier & Turner 2004). A better measure of $N(H_2)$ can be obtained from the $C^{18}O$. It is known to be optically thin and for the excitation temperatures observed, the intensities of the lower J transitions of $C^{18}O$ are not strongly dependent on gas excitation [see MT01 for a detailed discussion of $N(H_2)$ and its uncertainties in IC 342]. Hence we adopt optically thin $C^{18}O$ (1–0) and $[H_2/C^{18}O] = 2.9 \times 10^6$ ($[^{12}CO/C^{18}O] = 250$ [Henkel & Mauersberger 1993] and $[CO/H_2] = 8.5 \times 10^{-5}$ [Frerking et al. 1982]) when calculating the H_2 column densities, consistent with what is derived from the CO isotopomers. The lines observed in this study are also optically thin and have similar upper energy states, and thus their intensities vary with T_{ex} in step with $C^{18}O$, providing at least partial compensation for changing physical conditions. Moreover, $C^{18}O$ (1–0) has a higher critical density ($n_{crit} \simeq 2 \times 10^3$ cm^{-3}) than the optically thick CO and should have beam filling factors more similar to the lines presented here. If the highest critical density species are strongly subthermal, abundances may be somewhat overestimated. On the other hand, for these same high critical density species, it is expected that their

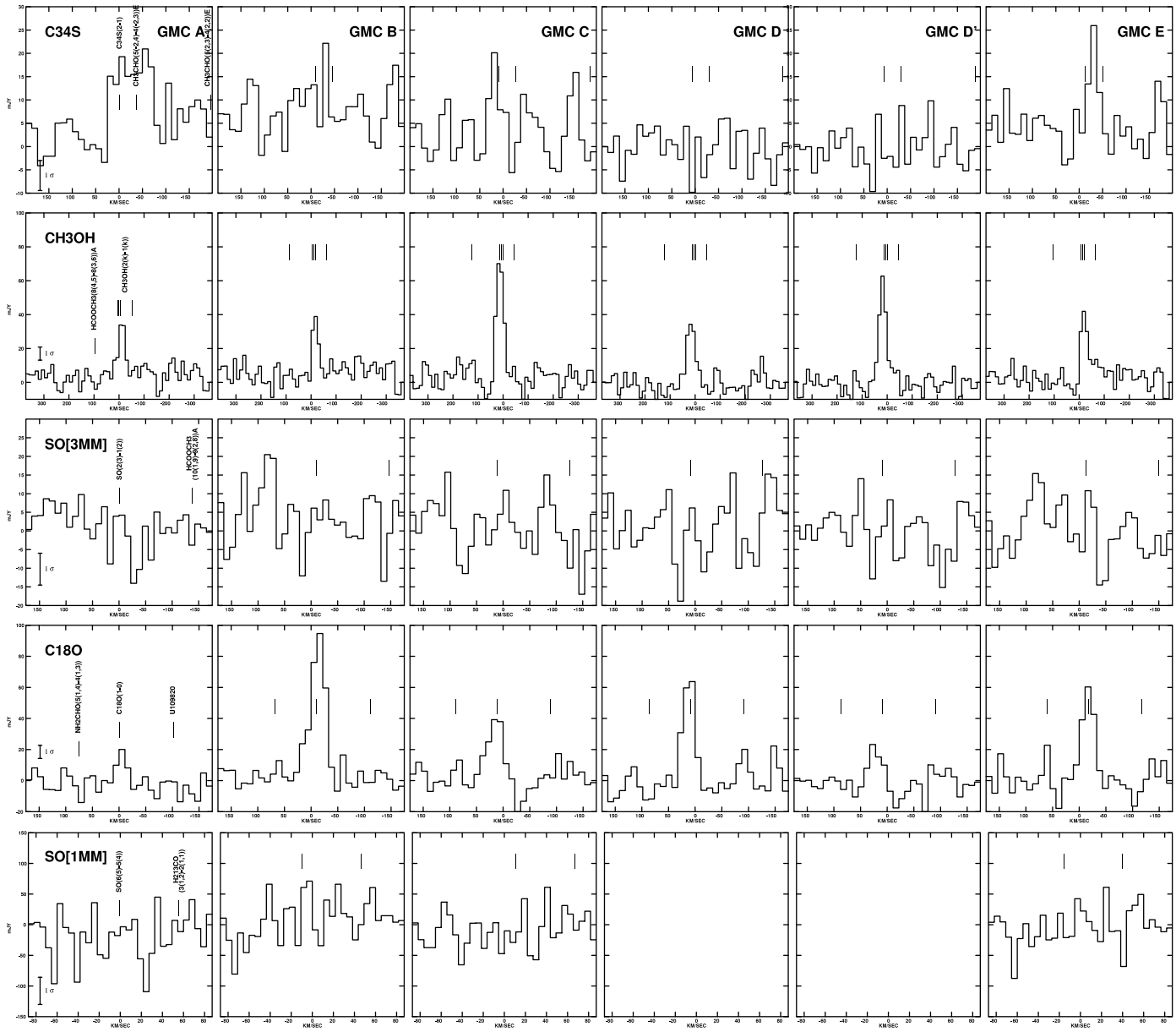

FIG. 5.—Same as in Fig. 4, except for the five remaining transitions.

emission will be more confined than $C^{18}O$ and hence underestimated locally. Together with the compensating effect of $C^{18}O$ (1–0) discussed above, we estimate that the column densities and fractional abundances are uncertain to at least a factor of 3, although the relative column densities—that is, the relative spatial distributions within the nucleus—are probably more reliable.

We now introduce each of the different molecular species that have been mapped and discuss their idiosyncrasies before we turn to the overall chemical picture in IC 342. Those who are already familiar with the molecules or are easily bored may skip to the next section.

C_2H, *ethynyl*.—This is the $J = 3/2–1/2$ fine-structure component of the $N = 1–0$ transition. C_2H is confined to the central ring, with a peak antenna temperature of $T_{mb} = 0.27$ K (Table 3) at GMC A. Figure 3 shows that the C_2H emission in GMC A does not originate from the main HCN peak but from its western side. C_2H is also brightest on the inner, starburst-lit face of GMC C, and it follows the Hα wisps (Fig. 1) between GMCs A and C. C_2H emission also appears in the central trough. The C_2H spectrum appears preferentially blueshifted toward the central regions of IC 342, but this may be an artifact of the presence of the $F = 1–0$ hyperfine component. At GMC A the line is strong enough to separate the $F = 1–0$ and $F = 2–1$ hyperfine components. Their ratio is 2, the value expected for optically thin, LTE excitation. The $F = 1–1$ component is not detected.

C_2H fractional abundances in Galactic cores are in the range of $(1–60) \times 10^{-10}$ (Wootten et al. 1980; Huggins et al. 1984; Watt 1983) and reach $\sim 2 \times 10^{-8}$ (Turner et al. 1999; Lucas & Liszt 2000) in Galactic diffuse clouds. In IC 342, a peak abundance of 3×10^{-8}, similar to Galactic diffuse clouds, obtains toward GMC A. Upper limits toward the other major GMCs are an order of magnitude lower, more like Galactic dense cores.

$C^{34}S$, *carbon monosulfide*.—The $J = 2–1$ rotational transition of $C^{34}S$ is expected to be optically thin. Like C_2H, $C^{34}S$ (2–1) emission is confined to the central-ring region and brightest toward GMC A ($T_{mb} = 0.16$ K). $C^{34}S$, however, lacks

TABLE 3

MEASURED INTENSITIES, LINE WIDTHS, AND CENTROIDS

GMC[a]	Molecule	T_b (K)	I_{mol} (K km s^{-1})	Δv (km s^{-1})	v_0 (km s^{-1})
A	C_2H	0.27 ± 0.05	15 ± 2	75 ± 8.5	19 ± 3.6
	HNC	0.50 ± 0.07	22 ± 3	40 ± 2.2	24 ± 1.0
	HNCO	≲0.078	≲3.6	...	...
	HC_3N	0.069 ± 0.02	4.1 ± 0.8	...	...
	N_2H^+	0.18 ± 0.03	8.9 ± 1	38 ± 5.7	26 ± 2.4
	CH_3OH	0.16 ± 0.04	6.4 ± 0.9	40 ± 6.7	24 ± 2.9
	$C^{34}S$	0.089 ± 0.02	8.5 ± 1	120 ± 38	−5.3 ± 16
B	C_2H	0.21 ± 0.05	8.3 ± 2	43 ± 7.3	4.8 ± 3.1
	HNC	0.62 ± 0.09	31 ± 5	30 ± 1.2	24 ± 0.6
	HNCO	∼0.11	5.3 ± 1	...	...
	HC_3N	0.088 ± 0.02	5.4 ± 0.9	20 ± 9.5	19 ± 4.3
	N_2H^+	0.19 ± 0.03	7.1 ± 1	23 ± 3.8	23 ± 1.5
	CH_3OH	0.15 ± 0.04	4.5 ± 0.9	25 ± 5.0	18 ± 2.2
	$C^{34}S$	∼0.053	3.6 ± 0.9	...	...
C	C_2H	∼0.11	7.2 ± 2	30 ± 9	33 ± 3.8
	HNC	0.47 ± 0.07	23 ± 3	40 ± 2.7	46 ± 1.1
	HNCO	0.23 ± 0.04	8.4 ± 1	30 ± 6.5	49 ± 2.7
	HC_3N	0.20 ± 0.03	8.4 ± 1	30 ± 5.8	52 ± 2.5
	N_2H^+	0.18 ± 0.03	7.6 ± 1	35 ± 6.2	48 ± 2.6
	CH_3OH	0.35 ± 0.05	15 ± 2	32 ± 2.8	48 ± 1.2
	$C^{34}S$	0.078 ± 0.02	3.6 ± 0.9	...	...
D	C_2H	<0.11	<1.5	...	...
	HNC	0.15 ± 0.03	8.4 ± 1	47 ± 7.8	47 ± 3.3
	HNCO	0.16 ± 0.04	3.9 ± 1	28 ± 5.8	54 ± 7.5
	HC_3N	<0.048	<1.5	25 ± 25	46 ± 13
	N_2H^+	0.11 ± 0.03	3.2 ± 0.8	35 ± 8.3	48 ± 3.5
	CH_3OH	0.12 ± 0.04	4.1 ± 0.9	38 ± 6.2	52 ± 2.7
	$C^{34}S$	≲0.048	≲1.8	...	...
D′	C_2H	<0.11	<1.5	...	...
	HNC	0.17 ± 0.03	6.7 ± 1	37 ± 5	50 ± 2
	HNCO	0.25 ± 0.04	7.2 ± 0.8	27 ± 3	56 ± 2
	HC_3N	∼0.04	∼1.1	26 ± 14	53 ± 6
	N_2H^+	0.13 ± 0.02	5.5 ± 1	40 ± 6	54 ± 3
	CH_3OH	0.26 ± 0.03	8.6 ± 1	31 ± 3	52 ± 1
	$C^{34}S$	<0.11	<1.5	...	...
E	C_2H	≲0.11	6.0 ± 2	47 ± 11	1.0 ± 4.6
	HNC	0.46 ± 0.07	18 ± 3	35 ± 2.2	18 ± 0.9
	HNCO	0.25 ± 0.04	5.8 ± 1	22 ± 3.3	15 ± 1.8
	HC_3N	0.084 ± 0.02	3.6 ± 0.8	37 ± 14	11 ± 5.8
	N_2H^+	0.21 ± 0.03	6.7 ± 1	28 ± 4.8	19 ± 2.0
	CH_3OH	0.16 ± 0.04	7.3 ± 1	30 ± 5	15 ± 2.1
	$C^{34}S$	0.089 ± 0.02	2.7 ± 0.9	25 ± 5.5	4.6 ± 2.5

NOTES.—T_b is the main-beam brightness temperature in kelvins based on the resolutions given in Table 1. I_{mol} is the peak integrated intensity in units of K km s^{-1} for the same resolution. Uncertainties are based on the larger of the rms noise or an estimated ≃15% absolute calibration errors for the temperatures and intensities, and 1 σ from the least-squared Gaussian fits for the velocity information. Upper limits represent 2 σ values.

[a] Peaks are based on the $C^{18}O$ data. See MT01 for coordinates, except for D′, which has coordinates $\alpha = 3^h46^m49^s.8$, $\delta = +68°5'59''.2$ (J2000.0).

TABLE 4

MOLECULAR ABUNDANCES IN IC 342

GMC	$N(H_2)$	C_2H	HNC	HNCO	HC_3N	N_2H^+	CH_3OH	$C^{34}S$	SO[a]
A	2.3	3(8)	2(9)	<1(9)	≲1(9)	5(10)	5(9)	2(9)	<7(9)
B	2.8	1(8)	2(9)	2(9)	1(9)	3(10)	3(9)	6(10)	<6(9)
C	3.2	1(8)	1(9)	2(9)	2(9)	3(10)	8(9)	5(10)	<5(9)
D	1.7	<4(9)	8(10)	2(9)	<6(10)	2(10)	4(9)	≲5(10)	<8(9)
D′	2.0	<3(9)	8(10)	3(9)	≲3(9)	5(10)	8(9)	<4(10)	<8(9)
E	3.5	∼7(9)	9(10)	1(9)	1(9)	2(10)	4(9)	∼3(10)	<5(9)

NOTES.—Format for entries is $a(b) = a \times 10^{-b}$, except for $N(H_2)$, which is in units of 10^{22} cm^{-2}. Each molecule is based on the assumptions of optically thin line emission with T_x also 10 K. Upper limits are 2 σ. Uncertainties are dominated by systematics and are at least a factor of 3 (see text for discussion of uncertainties). H_2 column densities are based on $C^{18}O$ (1–0) emission sampled at 6″ resolution. $T_x = 10$ K and an abundance of $[H_2/C^{18}O] = 2.94 \times 10^6$ are adopted (§ 3.2).

[a] In determining SO upper limits, a line width of 30 km s^{-1} has been assumed.

the eastern extension seen in C_2H. In general, $C^{34}S$ (2–1) avoids the density peaks traced in the Downes et al. (1992) HCN (1–0) image, although $C^{34}S$ also has a high critical density. As with C_2H, the northern extension appears predominately on the inner face of GMC C, toward the nuclear star cluster. The $C^{34}S$ line at GMC A is rather broader than seen in the other observed transitions and appears blueshifted like C_2H (Fig. 4).

For an $C^{32}S/C^{34}S$ isotopic abundance of 23 (e.g., Wilson & Rood 1994; however, see Chin et al. 1996), $X(C^{34}S) = (1-3)\times10^{-10}$ in Galactic dense cores (e.g., Wang et al. 1993; Morata et al. 1997; Lapinov et al. 1998) and diffuse/translucent clouds (Nyman 1984; Drdla et al. 1989; Lucas & Liszt 2002). In IC 342, we find $X(C^{34}S) = 2\times10^{-9}$ toward GMC A. The upper limits elsewhere are consistent with the typical Galactic values.

Convolving the $C^{34}S$ (2–1) interferometer data to the resolution of the single-dish map of the main CS isotopomer (Mauersberger et al. 1989) yields a morphology similar to that seen in the single-dish data, except with a less prominent northern peak. The CS (2–1)/$C^{34}S$ (2–1) intensity ratio toward the central peak is $\sim$8, while toward GMC C the intensity ratio increases to $\gtrsim$12. Assuming a Galactic $^{32}S/^{34}S$ abundance ratio of 23 implies an opacity of $\sim$2 in the main isotope toward GMC A and slightly lower opacities toward GMC C. However, recent observations suggest that in starburst nuclei, $C^{32}S/C^{34}S \sim 8-13$ (Wang et al. 2004; Martín et al. 2004). In this case, $C^{34}S$ (2–1) has low opacity everywhere in the nucleus.

HNC, *hydrogen isocyanide*.—The $J = 1-0$ line of the linear molecule HNC is the brightest of the observed lines with a peak antenna temperature of $T_{mb} = 0.62$ K, brighter even than $C^{18}O$ (1–0). HNC peaks at the starburst GMC B and is bright at all other labeled GMCs, with the possible exception of GMC E. The morphology of HNC (1–0) is similar to that of HCN (1–0) (Downes et al. 1992). HNC and HCN may be the best tracers of the dense gas distribution (§ 4). HCN emission, and presumably the dense gas, tends to arise on the clockwise (leading) side of the molecular arms when compared to ^{12}CO (1–0), an effect also seen in CO isotopomers (Wright et al. 1993; MTH00; MT01). The HNC peak at GMC C is shifted closer to the nucleus than the ^{12}CO (1–0). HNC (1–0) also peaks $\sim5''$ due east of GMC D, a feature not obvious in the map of HCN (1–0) (Downes et al. 1992). This location is bright in several other lines, particularly N_2H^+, CH_3OH, and HNCO. For the sake of reference, this location will be referred to as D′, and its position is given in Table 3.

HNC abundances are $(5-10)\times10^{-9}$ in Galactic dark clouds, and about an order of magnitude lower in clouds with massive star formation, including the Galactic center (Wootten et al. 1978; Blake et al. 1987; Hirota et al. 1998; Nummelin et al. 2000), or in diffuse and translucent clouds (Nyman & Millar 1989; Turner et al. 1997; Lucas & Liszt 2001). In IC 342, HNC abundances are fairly constant across the galaxy and consistent with that found in the Galactic center. Uncertain opacity effects could be important, although we view them as unlikely (§ 5.5).

N_2H^+, *diazenylium*.—We observed the ground ($J = 1-0$) rotational state of this linear molecule. The hyperfine splitting is much smaller than the observed line widths and is ignored. Emission from N_2H^+ is bright ($T_{mb} = 0.21$ K) and widespread, nearly matching HNC in extent. The higher resolution map shows that the N_2H^+ emission peaks between GMCs A and B, even though high-resolution images of CO do not show any local maxima at this location (Schinnerer et al. 2003). This peak is also seen in the maps of HC_3N, HNCO, and possibly HNC (Fig. 3), and in NH_3 (Ho et al. 1990), but in no other lines. This cloud appears only in nitrogen-bearing species, and so we label it "N" in Figure 3. On a larger scale, N_2H^+ is similar in morphology to NH_3, HNCO ($4_{04}-3_{03}$), and CH_3OH (2_k-1_k). All are bright toward GMC D′.

N_2H^+ abundances in Galactic dense cores range from 10^{-10} to 10^{-9}, with higher abundances in dark cores (Womack et al. 1992b; Benson et al. 1998). In diffuse and translucent clouds, N_2H^+ has fractional abundances well below 10^{-11} (Womack et al. 1992b; Turner 1995; Lucas & Liszt 2001). In IC 342 we find $X(N_2H^+) = 2\times10^{-10}$ up to 6×10^{-10} toward GMC D′. These abundances are up to an order of magnitude larger than the Galactic center values.

HC_3N, *cyanoacetylene*.—We mapped the $J = 10-9$ rotational transition of HC_3N. This molecule has the largest electric dipole moment and the highest upper energy state of the sample (Table 2). HC_3N emission is confined to the two GMCs associated with the youngest starbursts, GMCs B and C, with peak $T_{mb} = 0.20$ K at GMC C, where the molecular arms intersect the central ring. As with HNC and HCN (Fig. 3), the HC_3N peak toward GMC C is $\sim$one-half of a beamwidth closer to the nucleus than ^{12}CO (1–0). HC_3N emits faintly at cloud N.

Abundances of HC_3N toward Galactic cores are $X(HC_3N) \sim$ a few $\times10^{-11}$ to a few $\times10^{-10}$, with the cold cores toward the high end (Morris et al. 1976; vanden Bout et al. 1983; Chung et al. 1991). Translucent clouds have a similar range (Turner 1998). For IC 342, abundances peak toward GMCs C and D′ at 4×10^{-9}, somewhat higher than in cold Galactic clouds but much lower than the localized Galactic hot core values ($>10^{-7}$; e.g., de Vicente et al. 2000).

HNCO, *isocyanic acid*.—We observed the $K_{-1} = 0$ transition of the $J = 4-3$ rotational state of the prolate, slightly asymmetric top, HNCO. HNCO emission is extended, with peaks at GMCs C, D′, and N, and brightest at D′ at $T_{mb} = 0.25$ K. HNCO emits only weakly toward the starburst (GMC B) and is undetected at GMC A. This transition of HNCO, which has no hyperfine structure, has the narrowest line width of the sample, barely resolved in the 14 km s^{-1} wide channels. These line widths, narrow by extragalactic standards, are typical of Galactic GMCs with massive star formation, such as Sgr B2. Evidently, all galactic rotation has been resolved out at this spatial resolution and the velocity dispersion of individual clouds dominate.

Abundances of HNCO range from $X(HNCO) \lesssim 1\times10^{-9}$ up to 3×10^{-9} toward GMC D′. On $\sim$1–2 pc scales, Galactic massive dense cores have abundances of 10^{-9}, increasing to 10^{-8} as the line width of the cloud increases (Zinchenko et al. 2000). In translucent clouds abundances are $(1-3)\times10^{-9}$ (Turner et al. 1999), and up to more than 2×10^{-8} on subparsec size scales (Wilson et al. 1996; Kuan & Snyder 1996). HNCO abundances in IC 342, averaged over 50 pc scales, are similar to those on $\sim$1 pc scales for massive cores in the Galaxy.

CH_3OH, *methanol*.—We observed the blended set of 2_1-1_1 *E*, 2_0-1_0 *E*, 2_0-1_0 A^+, and $2_{-1}-1_{-1}$ *E* low-energy, thermal transitions of CH_3OH (hereafter designated the 2_k-1_k transition). CH_3OH (2_k-1_k) emission is as bright as $C^{18}O$ (1–0) and nearly as extensive as ^{13}CO (1–0)! The general morphology of CH_3OH is similar to that of $C^{18}O$ (1–0) following the ^{12}CO (1–0) emission, but favoring the leading edges of the nuclear arms. The brightest methanol emission comes from GMCs C and D′, with peak $T_{mb} = 0.35$ K at GMC C. An additional CH_3OH peak is seen even north of GMCs D/D′, a position only detected in methanol, $C^{18}O$ (1–0), and HNC (1–0). CH_3OH, like

TABLE 5
OTHER SELECTED TRANSITIONS

Molecule	Transition	ν (GHz)	T_{mb} (mJy beam^{-1})	GMC
HC_5N	33–32	87.8636	22 ± 7	B
HC_5N	35–34	93.1881	<13	...
$HCC^{13}CN$	10–9	90.6018	<10	...
C_2S	7_7–6_6	90.6864	<10	...
$^{13}C^{34}S$	2–1	90.9260	13 ± 5	C
CH_3CHO	5_{-24}–4_{-23} E	96.4256	[a]	[a]
$HCOOCH_3$	8_{45}–8_{36} A	96.7092	<16	...
NH_2CHO	5_{14}–4_{13}	109.7535	22 ± 8[b]	E
$H_2^{13}CO$	3_{12}–2_{11}	219.9085	<90	...
$C^{15}N$	2–1, 5/2–3/2, F = 3–2	219.734	<90	...
	...	93.132(4)	15 ± 6	B, C
	...	96.431(4)	19 ± 7[a]	B, C
	...	96.466(4)	14 ± 7	B, C, E
	...	109.221(4)	20 ± 9	B, E
	...	109.819(4)	20 ± 8	D
	...	109.839(4)	22 ± 8	D

NOTE.—Upper limits are 2 σ.
[a] Blended with $C^{34}S$ (2–1).
[b] Blended with SO_2 (17_{513}–18_{414}).

HNCO and N_2H^+, is bright toward GMC D′ and along the leading edge of the northern spiral arm. For a "hot gas" tracer, methanol is surprisingly weak near the starburst at GMC B, actually appearing as a local minima. GMC A is also weak in methanol.

Galactic methanol abundances range from 10^{-10} to 10^{-8}, depending on source size (e.g., Kalenskii & Sobolev 1994; Kalenskii et al. 1997; Minier & Booth 2002). Diffuse and dark cloud CH_3OH abundances are $(2-3)\times10^{-9}$ (Friberg et al. 1988; Turner 1998), as determined from thermal transitions. CH_3OH abundances in the envelope of Sgr B2 are $(3-10)\times10^{-9}$ (Nummelin et al. 2000). On smaller scales, methanol can be enhanced by factors of a few hundred over dark cloud values in shocks and outflows (e.g., Menten et al. 1986; Bachiller & Perez Gutierrez 1997). In IC 342, the observed range is $(3-8)\times10^{-9}$, similar to the envelope of Sgr B2. Multiline single-dish CH_3OH data obtain $T_{ex} \simeq 5-10$ K averaged over 200 pc size scales (Hüttemeister et al. 1997), suggesting that CH_3OH emission is not dominated by hot cores.

Nondetections, SO.—We attempted to image two transitions of SO, the 2_3–1_2 and 6_5–5_4 transitions. Upper limits (2 σ) of $I_{SO} < 1.5$ K km s^{-1} for the 2_3–1_2 line and $I_{SO} < 1.3$ K km s^{-1} for the 6_5–5_4 line are obtained. The SO abundance in Galactic dense cores is variable, ranging from $X(SO) \sim 5\times10^{-11}$ up to 1×10^{-7}, with enhancements seen toward dark clouds and hot cores (Gottlieb et al. 1978; Rydbeck et al. 1980; Blake et al. 1987) and in diffuse or translucent clouds $(2-30)\times10^{-9}$; Turner 1995; Heithausen et al. 1995; Lucas & Liszt 2002). In IC 342, the upper limits for SO of $(5-8)\times10^{-9}$ are not strongly constraining.

Table 5 presents the limits for fainter transitions within the bandwidth of the spectrometer. We note that the broadening of $C^{34}S$ (2–1) could be due to contamination from the $5_{-2,4}$–$4_{-2,3}$ E transition of acetaldehyde (CH_3CHO) at 96.426 GHz. The Turner (1989) 3 mm survey finds this transition to be approximately one-fifth the brightness of $C^{34}S$ (2–1) in Sgr B2. In IC 342, it would have to be comparable in brightness to $C^{34}S$ (2–1) to explain the line width, which is unlikely. A 3 σ feature is also seen in the $C^{18}O$ (1–0) bandpass, matching the frequency of the $5_{1,4}$–$4_{1,3}$ E transition of formamide (NH_2CHO) at 109.754 GHz. In the Turner (1989) survey of Sgr B2 this transition has a brightness one-fifth that of the $C^{18}O$ (1–0) line. Toward GMC E, where the feature is brightest, the observed ratio is ~1/3. Therefore, it is possible that this feature is NH_2CHO. CH_3CHO and NH_2CHO have yet to be detected in external galaxies. These deep interferometric observations suggest that these two aldehydes may be worth a dedicated search.

In the rest of the paper, we will omit the transition notations for the molecules to facilitate the exposition. The reader should be aware that the correlations that we investigate may be a function of the energy level and excitation, i.e., the specific transition, as well as the chemistry (§ 5).

4. UNDERSTANDING THE MOLECULAR MAPS: PRINCIPAL-COMPONENT ANALYSIS

The maps give a picture of the astrochemistry of the molecular clouds in the nuclear region of IC 342. To begin to interpret these maps, we need to establish similarities and differences between the molecules. The correlations will reveal trends in what governs the chemistry, which in turn can reveal the physical characteristics and forces within the galaxy that create these conditions.

To quantify the morphologies of the molecular maps and star formation, we apply a principal-component analysis (PCA). PCA is a common technique (e.g., Murtage & Heck 1987; Krzanowski 1988; Everitt & Dunn 2001; Wall & Jenkins 2003, chap. 4.5) used to reduce the dimensionality of a data set. It is useful in identifying a small linear combination of data points that convey a significant percentage of the information of the whole data set. The PCA simplifies the picture of molecular distribution, reducing a large amount of information to a few images, providing an excellent framework within which to study the complex variations in molecular properties in IC 342.

For a description of PCA applied to multitransition molecular maps, see Ungerechts et al. (1997). Each pixel in each map is treated as a separate data point in an $x \times y \times n$ dimensional space, where x and y are the number of pixels along the corresponding axis of the maps, and n is the number of maps

TABLE 6
PCA Correlation Matrix

Maps	^{12}CO	$C^{18}O$	3 mm	C_2H	$C^{34}S$	CH_3OH	HC_3N	HCN	HNC	HNCO	N_2H^+
^{12}CO	1.0	...	...	...	...	...	...	...	...	...	...
$C^{18}O$	0.82	1.0	...	...	...	...	...	...	...	...	...
3 mm	0.65	0.76	1.0	...	...	...	...	...	...	...	...
C_2H	0.53	0.62	0.76	1.0	...	...	...	...	...	...	...
$C^{34}S$	0.38	0.39	0.48	0.50	1.0	...	...	...	...	...	...
CH_3OH	0.75	0.80	0.67	0.49	0.21	1.0	...	...	...	...	...
HC_3N	0.60	0.71	0.85	0.57	0.30	0.68	1.0	...	...	...	...
HCN[a]	0.65	0.75	0.90	0.74	0.49	0.64	0.77	1.0	...	...	...
HNC	0.76	0.85	0.94	0.79	0.49	0.72	0.81	0.91	1.0	...	...
HNCO	0.67	0.75	0.58	0.42	0.19	0.78	0.57	0.57	0.66	1.0	...
N_2H^+	0.73	0.81	0.75	0.59	0.42	0.71	0.68	0.74	0.82	0.69	1.0

[a] Data from Downes et al. (1992). The data were taken at the Plateau de Bure Interferometer and hence have a slightly smaller primary beam.

included. The "cloud" of samples is then projected onto an axis such that the variance along that axis is a maximum. This projection corresponds to the first principal component. The task is repeated, subject to the constraint that each successive projection is orthogonal to all previous projections. Each projection, the principal components or eigenvectors, will contain decreasing fractions of the total data variance (assuming that there is some correlation in the maps). As long as the first few principal components contain a significant fraction of the variability in the data, the entire data set can be adequately described by just these few principal components.

To calculate the principal components for IC 342, the line maps were convolved to the same geometry and beam size (6″), normalized, and mean-centered. Eleven maps, ^{12}CO (1–0), $C^{18}O$ (1–0), HCN (1–0) (Downes et al. 1992), and 3 mm continuum (MT01), plus the seven detected transitions, were sampled at 1″ intervals over the central 32″ × 62″, making up a 20,824 element data space. The algorithm used to calculate the principal components is essentially that of Murtage & Heck (1987). The results are displayed in Tables 6 and 7 and in Figures 6 and 7.

The correlation matrix resulting from the PCA (Table 6) indicates that all molecules are at least partially correlated. This is also represented by the most significant correlation, component PC1 (Fig. 6*a*). HCN and HNC are the most tightly correlated of the molecules. $C^{18}O$, N_2H^+, HCN, and HNC have large projections onto PC1 but small projections onto PC2 and PC3 (and the PC2 and PC3 projections of $C^{18}O$ and HNC have opposite signs). Since HNC is expected to trace the distribution of dense quiescent gas and $C^{18}O$ the column density, it would appear that PC1 represents the density-weighted average column density map of IC 342. This also agrees with the general appearance of PC1. In fact, the PC1 map is basically an average of the $C^{18}O$ and HNC maps. PC1 accounts for approximately two-thirds of the variance in the data, and all species have large projections onto PC1. Variations in density-weighted column density therefore explain much of the overall morphology of the chemical species, as one might expect. Molecules are found in molecular clouds. The molecule N_2H^+ projects almost exclusively onto PC1. N_2H^+ in the Galaxy is considered a good "quiescent gas" tracer, and that also appears true in the nucleus of IC 342.

HNC, another molecule with a large PC1 projection, is the molecule most closely correlated with the 3 mm continuum. Of all of the detected transitions, HNC has the highest critical density and is most heavily weighted toward regions of high density, and not just high column density. Thus the 3 mm continuum is very closely associated with the dense gas. This extends the findings of Gao & Solomon (2004) based on their studies of global HCN fluxes in galaxies down to GMC size scales. However, the correlation of dense gas with star formation, while excellent, is not perfect; we discuss this in § 5.

The next principal component, PC2, characterizes the correlations remaining once density-weighted column density

TABLE 7
PCA Eigenvectors

	PCA Component						
Molecule	1	2	3	4	5	6	7
^{12}CO	0.30	0.19	0.36	0.075	−0.69	0.084	0.27
$C^{18}O$	0.33	0.16	0.17	0.063	−0.14	−0.039	0.009
3 mm	0.33	−0.18	−0.30	−0.12	0.032	0.032	0.080
C_2H	0.28	−0.37	−0.16	0.75	0.064	0.13	−0.25
$C^{34}S$	0.18	−0.62	0.62	−0.33	0.20	0.21	0.070
CH_3OH	0.30	0.38	0.076	0.003	0.021	0.44	−0.56
HC_3N	0.30	0.026	−0.44	−0.54	0.034	0.21	−0.16
HCN	0.33	−0.19	−0.23	−0.038	0.024	−0.082	0.43
HNC	0.35	−0.11	−0.13	−0.058	−0.074	−0.10	0.18
HNCO	0.27	0.43	0.21	0.11	0.67	0.10	0.39
N_2H^+	0.32	0.078	0.15	−0.089	0.090	−0.81	−0.39
Eigenvalue percentage	70	10	5.8	3.4	2.7	2.4	1.8

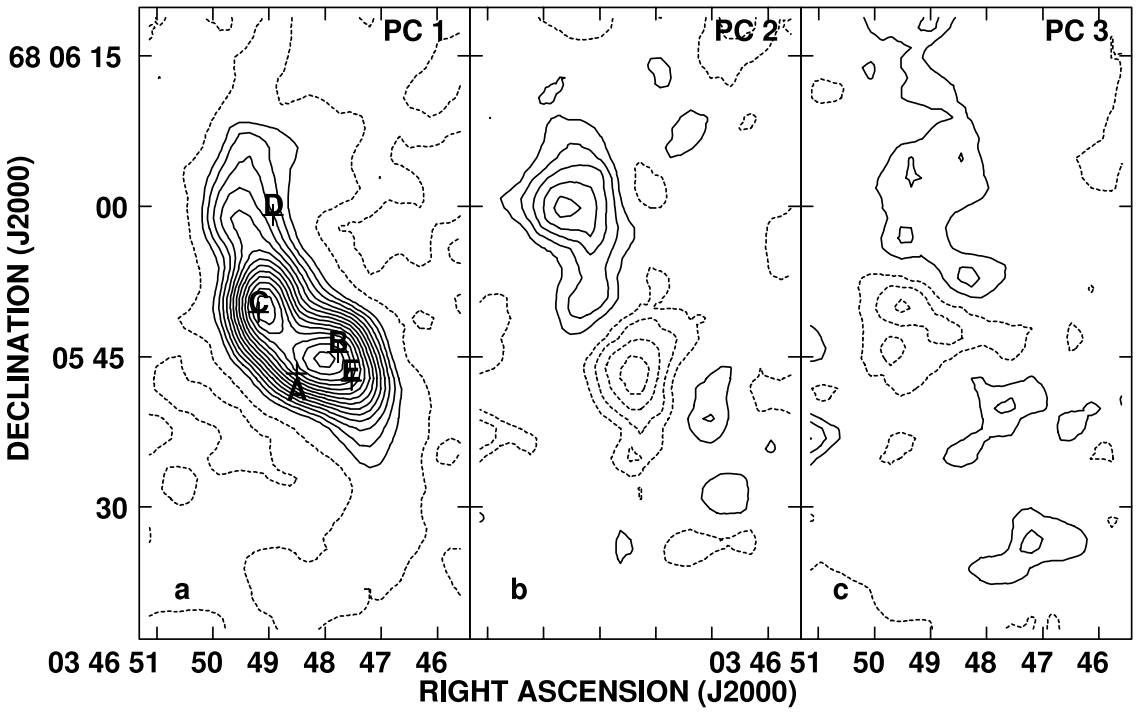

FIG. 6.—Maps of the first three principal components of the molecular distribution.

effects are taken into account. As shown in Figure 6*b*, PC2 distinguishes between molecules that peak at GMC A and those that are extended along the northern arm, particularly those peaking at GMC D′. HNCO and CH_3OH, which are found along the northern arm and are absent in GMC A, have the largest positive projections onto PC2 and are well correlated. C_2H and $C^{34}S$ have large negative projections onto PC2, appearing almost exclusively at GMC A. These groups are anticorrelated in the sense that clouds bright in C_2H and $C^{34}S$ show little HNCO and CH_3OH emission, and vice versa. These differences suggest that these two groups—defined by the northern arm and GMC A locations—represent distinct types of chemistry. We discuss the chemistries of the GMC A versus northern arm/GMC D′ groups below. HC_3N, 3 mm continuum, and N_2H^+ are largely independent of PC2, indicating that their emission is not strongly influenced by the different chemical conditions of GMC A versus northern arm/GMC D′.

PC3 is of less significance than the previous two correlations. PC3 distinguishes between GMC C (particularly between upstream [^{12}CO and $C^{34}S$] and downstream [HC_3N and 3 mm] species) and between GMCs C and D. PC3 thus hints at being connected with the distribution of massive star formation.

5. SPATIALLY RESOLVED CHEMISTRIES IN THE NUCLEUS OF IC 342

The large variations in spatial morphology observed for the different molecules across the central half kiloparsec of IC 342 are caused by either differences in emissivity (excitation) or abundances (chemistry). In this section we discuss the possible influences on the molecular emission that could lead to the observed variations.

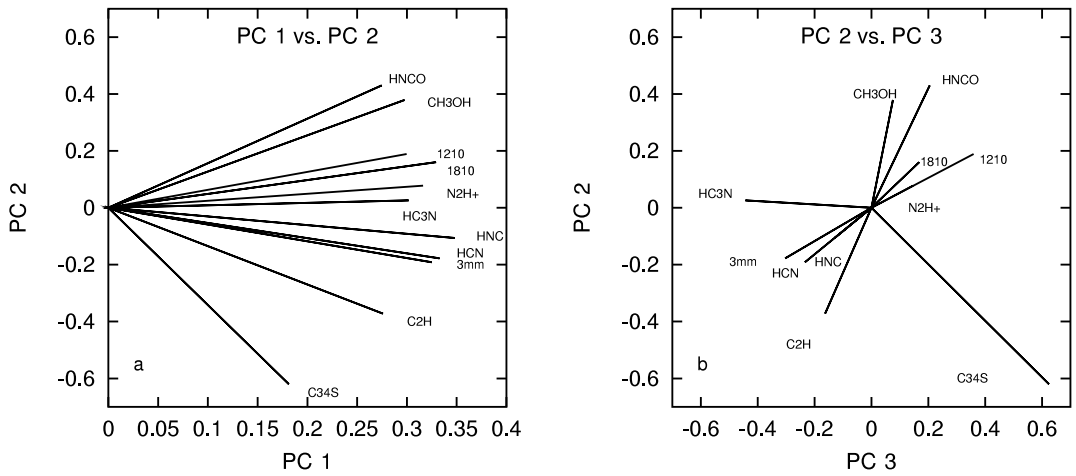

FIG. 7.—Projections of each species on the first three principal components. (*a*) Each transition projected onto the plane defined by the first and second principal components. (*b*) Each transition projected onto the plane defined by the second and third principal components. The figure is plotted in such as way that (*b*) may be visualized as looking down the *x*-axis of (*a*) from the right.

5.1. *Are Differences between the Molecular Species Due to Excitation?*

The molecules of our sample have lower opacities, higher critical densities, and larger partition functions than CO, and so these lines are more sensitive to changes in excitation due to variations in density that can affect emissivity. Since we already know a fair amount about cloud conditions in IC 342 from the 1–0 and 2–1 lines of the CO isotopomers, we can investigate how important excitation is to the emissivities of these molecules. All of the detected lines have similar upper level energies and thus behave similarly to changes in excitation temperature T_{ex} (see Table 2). Significant variations in T_{ex} as traced by $C^{18}O$ are not seen, with a range of temperatures across the nucleus of 7–15 K, except for a small region toward the starburst (GMC B). Since the excitation properties are similar and most of the gas is at a relatively uniform excitation temperature anyway, T_{ex} is not the major cause of the spatial differences between the molecules.

Critical density can also play a role in emissivity. The range of electric dipole moments for the observed species of $\mu_0 = 0.8$ (C_2H) to 3.73 (HC_3N) corresponds to a factor of $\sim$20 in critical density (>1000 if one counts CO). The CO isotopomers indicate that volume densities of the GMCs are $\gtrsim 10^4$ cm^{-3} (MT01). At this density, transitions with the highest critical density should have the most limited extent. However, we find that there are extended and confined species at both lower critical densities (CH_3OH vs. C_2H) and intermediate critical densities (HNCO vs. $C^{34}S$), as well as the highest critical densities (N_2H^+ vs. HC_3N). We conclude that densities in the GMCs are $\sim 10^5$ cm^{-3}, high enough to (at least partially) excite all of the molecules everywhere across the nucleus, except perhaps HC_3N and N_2H^+, which have the very highest critical densities.

Although variations in density and temperature are not the primary forces determining the appearance of the maps of Figure 2, there may be regions where they play a role. GMC A is genuinely different from the other GMCs, in spite of its similarity in CO and HCN. The first hints that GMC A was different came from the temperature map made using $C^{18}O$ (MT01). GMC A is a localized "hot spot," with $T_{ex} \simeq 15$ K, higher than the 10 K we adopt here. The species with intensities most sensitive to changes in T_{ex}, HNCO and CH_3OH, would be the most affected by a higher temperature; the observed weakness of HNCO and CH_3OH in GMC A could be due to depopulation of low-lying transitions. This effect is also possible for the localized maxima of CH_3OH toward GMC B. The second instance in which excitation appears to play a role is in HC_3N, which is closely confined to the starburst sites. This may indicate that the sites of the strongest star formation are the locations with the highest combined density and temperature.

Aside from these exceptions, variations in gas physical conditions do not appear to determine the widespread morphological changes seen in the chemical maps. Since the morphology of the maps is not explained completely in terms of changes in physical conditions, variation in the chemistry—relative molecular abundances—must be important.

5.2. *Do the Maps Reflect Chemical Timescales?*

One difference between molecular clouds of our Galactic disk and the clouds we observe in the nucleus of IC 342 is timescale. Dynamical timescales are shorter in galactic nuclei than they are in disks. Chemical models show that steady state chemistry obtains after 10^6–10^7 yr (e.g., Herbst & Klemperer 1973; Prasad & Huntress 1980) and that abundances of molecules tend to fall into two categories. "Early time" molecules, typically radicals and hydrocarbons—in general species descending from C or C^+—are abundant early and get burned into CO and more complicated species as time passes. "Late time" molecules, such as N_2H^+, NH_3, and SO, form from slower neutral-neutral reactions or are quickly destroyed by abundant C and C^+. Early-time species tend to peak by $\sim 10^5$ yr, whereas late-time species reach their peak at steady state (>10^6 yr) (e.g., Graedel et al. 1982; Watt 1983; Millar & Nejad 1985). In the disk of our Galaxy, these timescales are much shorter than the time between spiral arm passages, so that steady state chemistry is expected in the absence of other disturbances.

In galactic centers, orbital timescales are short enough to rival chemical timescales. Based on the rotation curve in the nucleus of IC 342 (Turner & Hurt 1992), $\tau_{GMC} \lesssim 3$ Myr at the central ring, 7 Myr at 20″, and 10 Myr at the edge of the molecular arms. The arms seen in IC 342 are known to have strong noncircular and shearing motions, the expected response to a barred potential (Ishizuki et al. 1990; Turner & Hurt 1992; Schinnerer et al. 2003). It is likely that upon approaching/entering the arms, molecular clouds are either torn apart by the strong velocity gradients along the arm or are shocked due to cloud-cloud collisions, and this will happen for a significant fraction of the orbit, or every $\sim$a few $\times 10^5$ cm^{-3}. The "chemical clock" of the molecular clouds could well be reset after traversing the arms. Molecular clouds near the dynamical center of the galaxy may not be able to establish chemical equilibrium between arm passages; clouds farther out can potentially achieve equilibrium. A transition from early-time species to late-time species as galactocentric radius increases will then be manifested.

The early-time species C_2H and HC_3N are confined to the central-ring region. However, other species such as HNC and CH_3OH (early time if produced by gas-phase reactions; e.g., § 5.4) are extended. N_2H^+, the most prominent late-time species detected, is actually brightest toward the central ring. Therefore, we conclude that time-dependent chemistry is not the dominant effect causing the chemical differences between the clouds in IC 342. With the short orbital timescales it is likely that early-time chemistry is the relevant chemistry over the whole region, although in this context the brightness of the late-time molecule N_2H^+ is surprising. In the next section we show that photodissociation region (PDR) chemistry may also create the appearance of early-time chemistry in this region.

5.3. *The Effects of a High Radiation Field: PDR Chemistry and the Cloud A Peakers* C_2H *and* $C^{34}S$

PDRs are widely believed to be responsible for many chemical properties of molecular clouds. IC 342 has active nuclear star formation, with $L_{OB} \sim 10^8\ L_\odot$, and a slightly older (>10 Myr) nuclear star cluster. Clearly PDR chemistry will be important; however, is it a dominant driver of the chemistry in IC 342?

The observed molecules most affected by PDR chemistry are C_2H and the sulfur-bearing species such as $C^{34}S$. The spatial distributions of these molecules are distinct from the others (Fig. 7), and it is likely that C_2H and $C^{34}S$ emission trace the molecular clouds that are experiencing particularly high radiation fields. We discuss the chemistry and detailed distribution of each below.

5.3.1. C_2H

The gas-phase chemistry of C_2H follows two main pathways. One is dissociative recombination with hydrocarbon ions:

$$C_2H_2^+ + e^- \rightarrow C_2H + H, \quad (2)$$

$$C_2H_3^+ + e^- \rightarrow C_2H + 2H/H_2, \quad (3)$$

where $C_2H_2^+$ and $C_2H_3^+$ are built up from reactions of the form (e.g., Wootten et al. 1980; Watt et al. 1988; Sternberg & Dalgarno 1995; Turner et al. 2000)

$$C^+ + CH_n \rightarrow C_2H_2^+ + H/H_2. \quad (4)$$

The second pathway involves the direct photodissociation of acetylene (C_2H_2), which also forms from reaction (3) (e.g., Truong-Bach et al. 1987; Fuente et al. 1993; Heikkilä et al. 1999). C_2H is destroyed primarily by photodissociation at A_v ($\sim$1 mag) and by reactions with O and C^+ at $A_v \sim 5-6$ mag (e.g., Wootten et al. 1980; Watt et al. 1988; Turner et al. 2000). C_2H should be abundant where C^+ and FUV photons are profuse. In the Galaxy, C_2H abundances of $X_{C_2H} \gtrsim 10^{-8}$ are observed in the diffuse ($A_V \sim 1-5$ mag) PDR gas (e.g., Fuente et al. 1993; Heikkilä et al. 1999; Lucas & Liszt 2000).

In IC 342, C_2H emission is confined to within 40 pc of the dynamical center, where the radiation field is high because of current star formation and the 60 Myr nuclear star cluster. C_2H is bright even in the central molecular "trough" coincident with the nuclear star cluster (Fig. 3). Except in GMC A, C_2H emission avoids the density peaks traced by HCN. In GMCs C and possibly B, C_2H emission peaks toward the side of the GMC facing the nuclear cluster. (This could also be true for GMC A, which is probably viewed face-on and therefore difficult to judge.) C_2H appears to arise from cloud surfaces illuminated by the nuclear star cluster and not by the young IR/radio star-forming regions. The influence of the IR/radio star-forming regions may be localized and minimized because these young stars are still deeply embedded where their photons remain trapped. GMC A, which is the brightest in C_2H, is the closest cloud to the nuclear cluster. Apparently photons can penetrate GMC A more effectively than the other clouds. Perhaps GMC A is more diffuse than the other GMCs, in spite of its bright HCN emission.

5.3.2. *Sulfur-bearing Molecules:* $C^{34}S$

Reactions of S and S^+ with hydrogen are endothermic, so sulfur chemistry is not initiated through hydrides. For CS, formation is primarily via

$$HCS^+ + e^- \rightarrow CS + H, \quad (5)$$

where HCS^+ comes from

$$S^+ + CH/C_2 \rightarrow CS^+ + H/C \quad (6)$$

and

$$C^+ + SO \rightarrow CS^+ + O, \quad (7)$$

followed by reactions with H_2. The reaction

$$C + SO \rightarrow CS + O \quad (8)$$

can also be important in the formation of CS, particularly when there is a large SO abundance. At low A_v, reaction (6) is dominant in the formation of CS^+, while at large A_v reaction (7) is dominant. CS is destroyed by reactions with atomic O and He^+ (H_3^+, and HCO^+ also destroy CS but the products are rapidly recycled back into CS) and by photodissociation. Photodissociation is dominant in the destruction at low A_v (e.g., Drdla et al. 1989; Turner 1996).

SO is considered a late-time species built up through the neutral-neutral reaction

$$S + OH \rightarrow SO + H \quad (9)$$

and destroyed by reactions (7) and (8) in C/C^+-rich environments. In environments where carbon has yet to be locked into CO, SO tends to be burned into CS. Therefore, the abundance ratio [SO]/[CS] is lower at early times ([SO]/[CS] $\ll 1$) in regions of high C/O elemental abundance and low A_v than it is at late times ([SO]/[CS] $\gtrsim 10$) (e.g., Swade 1989; Bergin et al. 1997; Nilsson et al. 2000).

$C^{34}S$ peaks in the central trough and near GMC A. The CS abundance may be enhanced in these regions through the increase in S^+ associated with a high UV flux from the nuclear cluster. The CS abundance can be approximated as (e.g., Sternberg & Dalgarno 1995)

$$X_{CS} \sim \frac{k_{CH} X_{S^+} X_{CH} + k_{C_2} X_{S^+} X_{C_2}}{(G_0/n_{H_2}) k_\gamma (CS)}. \quad (10)$$

If S is undepleted and mostly ionized as expected at modest A_v, then for values of $k_{CH} \simeq 6.3 \times 10^{-9}$ cm^3 s^{-1}, $k_{C_2} \simeq 8.1 \times 10^{-10}$ cm^3 s^{-1}, $k_\gamma \simeq 2 \times 10^{-10} \exp(-2A_v)$ s^{-1}, and $[CH] \sim [C_2] \sim 10^{-8}$ (Drdla et al. 1989), the observed CS (23*$C^{34}S$) abundances of a few $\times 10^{-8}$ are obtained for $A_v \simeq 3$, when $G_0 = 320$ (Israel & Baas 2003) and $n_{H_2} = 10^4$ cm^{-3}. This is consistent with the observed $C^{34}S$ morphology.

The SO/(23*$C^{34}S$) intensity ratio is everywhere less than 0.7 and less than 0.1 (2 σ) toward GMC A. While not strongly constraining, this shows that SO is not enhanced in IC 342's nucleus and is consistent with S molecule formation in a C/C^+-rich environment.

In the PCA analysis, $C^{34}S$ is the most anomalously distributed molecule of all (Fig. 7), with the lowest correlation coefficients with any other molecule. We suggest that this may be due to the abundance distribution of ionized sulfur (S^+). In diffuse PDR cloud edges, sulfur should be relatively undepleted and ionized (e.g., Lepp et al. 1988). The bright $C^{34}S$ emission toward GMC A and toward the edges of GMCs B and C is consistent with this model. If so, then the GMC A cloud is relatively well illuminated. In dense clouds, sulfur should be depleted onto the grains, and $C^{34}S$ comparatively faint. This is the case for the GMCs other than A and the edges of B and C toward the nuclear cluster. CS depletion in the denser regions of dark clouds is well established in the Galaxy, although on a much more local scale (e.g., Bergin et al. 2001; Di Francesco et al. 2002).

5.4. *Shocks and Gas-Grain Chemistry in IC 342: The Northern Arm Peakers* CH_3OH, HNCO

The pronounced spiral morphology in the nucleus of IC 342 indicates that shocks are likely to be present, both in the spiral arms and where the spiral arms meet the nuclear ring. Shocks

can influence the chemistry of molecular clouds by raising gas temperatures, but they also affect the chemistry by liberating molecules formed through the processing of grain mantles. Two molecules believed to be produced by grain processing are CH_3OH and HNCO.

5.4.1. CH_3OH

The gas-phase chemistry of methanol is simple. The only formation mechanism is radiative association of $CH_3^+ + H_2O$ to form $CH_3OH_2^+$, followed by dissociative recombination (Millar et al. 1991; Turner 1998). This formation mechanism is too slow to produce methanol relative abundances greater than $X(CH_3OH) \sim (1-3) \times 10^{-9}$ (Lee et al. 1996). Abundances in Galactic star-forming regions can reach up to $\sim 10^{-7}$ (e.g., Menten et al. 1986), and interstellar ice mantles are rich in methanol, $X(CH_3OH) \sim 10^{-6}$ (Schutte et al. 1991). The high abundance of the methanol is thus believed to arise from hydrogenation of CO on grain surfaces. Methanol is expected to trace warm ($T_k \gtrsim 90$ K) molecular gas where mantles have been evaporated.

In IC 342, methanol emission is widespread and bright and traces out the leading edges of the two molecular arms. If methanol were produced by the evaporation of grain mantles by warm molecular gas, then $T_k \gtrsim 90$ K would be required. Instead, $T_k \lesssim 50$ K (§ 3.2) and $T_{ex}(CH_3OH) \sim 10$ K are indicated (Hüttemeister et al. 1997) for the nuclear region. Despite the cool temperatures, the fractional abundance of CH_3OH is uniformly at or above $X(CH_3OH) \sim 3 \times 10^{-9}$ (Table 4). A second method of injecting a large amount of grain mantle material back into the ISM is through shock disruption of grains. Grain mantle material can be liberated either by the localized heating due to the shock or directly via grain disruption (e.g., Sandell et al. 1994; Bachiller & Perez Gutierrez 1997; Bergin et al. 1998). In mild shocks ($v_s \lesssim 10$ km s^{-1}), mantles of grains can be liberated without destroying the molecules in the process (e.g., Bergin et al. 1998). In order to be relevant for these observations, the shocks must operate coherently over several tens of parsecs in order to generate noticeable enhancements on the observed scales. Shocks due to local phenomena such as outflows from massive stars likely do not influence enough of the molecular gas to explain the elevated abundances unless there are a very large number of them.

Large-scale shocks due to orbital dynamics are the most plausible explanation for the bright methanol emission. The central region of IC 342 must have a barred potential to explain the overall molecular morphology. Noncircular orbital motions and highly supersonic changes in velocity direction are observed, particularly in the northern arm (e.g., Turner & Hurt 1992). Orbital shocks associated with cloud-cloud collisions would be expected, although the exact nature of these shocks would depend on the strength and geometry of the magnetic fields. We expect shock processing of grains to be most important along the arms, at the intersections of the molecular arms and the central ring (the x_1-x_2 orbital intersections: GMCs B and C) and at the bar ends where the molecular gas piles up and collides with the existing molecular gas in the arms (GMC D/D′). All of these locations are sites of bright methanol emission. While star formation at GMCs B and C complicates the interpretation at the x_1-x_2 orbital intersections, the enhanced methanol abundance toward GMC D/D′ is almost certainly due to shocks resulting from molecular gas from the southern arm, "spraying" off the central ring and colliding with the gas already present in the northern arm.

5.4.2. *The Enigmatic* HNCO

The chemistry of HNCO is poorly understood. The distribution in IC 342 and its correlation with other northern arm peakers such as methanol give interesting insights on the chemistry of HNCO.

It has been proposed that the excited K ladders ($K_{-1} > 0$) of HNCO are excited by FIR radiation because their critical densities are prohibitively high for collisional excitation (e.g., Churchwell et al. 1986; Wilson et al. 1996; Blake et al. 1996). The situation is less clear for the $K_{-1} = 0$ transitions observed here because the critical densities are lower. Rapid b-type transitions from $K_{-1} > 0$ to $K_{-1} = 0$ states can thermalize the level populations at the 330 μm ($K_{-1} = 1-0$) and 110 μm ($K_{-1} = 2-1$) radiation temperatures, but the lower critical densities make collisional excitation more relevant. In both Sgr B2 and OMC-1, the low-lying $K_{-1} = 0$ transitions have higher column densities and lower rotational temperatures as compared to the excited K ladders (Churchwell et al. 1986; Blake et al. 1987). Derived abundances of HNCO ($K_{-1} = 0$) can be high, and emission much more widely distributed than found for the $K_{-1} \neq 0$.

In IC 342, HNCO is not well correlated with either molecular column density traced by ^{13}CO, dense gas traced by HCN, or massive star formation traced by 3 mm continuum. One would expect that if the dominant excitation mechanism for HNCO were FIR pumping, it would tend to be found near regions of active star formation and large gas column density. That it is not arising from GMCs B and C argues against excitation mechanisms involving the FIR radiation field. We conclude that the 3 mm $K_{-1} = 0$ transitions of HNCO do not trace the FIR radiation field in IC 342. The HNCO emission appears to be governed by abundance variations rather than excitation.

Iglesias (1977) considered the possibility that HNCO is formed from electron recombination of H_2NCO^+, which has been produced by ion-molecule reactions between NCO^+ and H_2. He found that this model fell short of the observed abundances by an order of magnitude. Turner et al. (1999) suggest that the dominant formation mechanism is through

$$\begin{aligned} CN + O_2 &\rightarrow NCO + O, \\ NCO + H_2 &\rightarrow HNCO + H \end{aligned} \qquad (11)$$

and destroyed predominately by reactions with H_3^+ and He^+. For abundances $X(HNCO) \lesssim 10^{-9}$ typical of the translucent clouds being studied, they argue that gas-phase reactions alone appear necessary to explain the observed abundances. While the first reaction step is rapid, the second possesses a significant activation barrier ($\sim$1000 K), and therefore the above reaction scheme may be too slow at typical ISM temperatures. In addition, O_2 is notoriously underabundant in the Galactic ISM (e.g., Bergin et al. 2000; Goldsmith et al. 2000), hence the abundance of NCO is very poorly known. So as it stands, gas-phase chemistry alone may able to generate $[HNCO/H_2] \sim 10^{-10}$ to 10^{-9}, but the matter remains unsettled.

Gas-grain chemical models have no trouble producing large abundances of HNCO. Chemical models find that significant amounts of HNCO [$X(HNCO) \sim 10^{-6}$] are formed in ice mantles by reactions such as CO (grains) + N (grains) + H (grains) $\rightarrow$ HNCO, C (grains) + N (grains) $\rightarrow$ CN (grains), CN (grains) + O (grains) $\rightarrow$ NCO (grains), and NCO (grains) + H (grains) $\rightarrow$ HNCO (Hasegawa & Herbst 1993). HNCO can also be formed

by reactions of NH_3 (and its daughter products) with CO (Hudson & Moore 2000). Observers of ice mantles have often ascribed the so-called 4.62 μm XCN feature to the ion OCN^- (e.g., Grim & Greenberg 1987; Demyk et al. 1998; Novozamsky et al. 2001), which forms either from UV photolysis of $CO + NH_3$ (e.g., Grim & Greenberg 1987; Schutte & Greenberg 1997) or by acid-base reactions between HNCO and NH_3 (e.g., Keane et al. 2001). In either case, the presence of this feature has been taken as evidence that HNCO is an abundant constituent of interstellar ices (e.g., van Dishoeck & Blake 1998; van Broekhuizen et al. 2004). If so, then as with SiO and CH_3OH, it is reasonable to expect that HNCO abundances may also be enhanced in shocked regions.

Observational evidence is mounting for a shock tracer interpretation for the production of HNCO. (1) In Sgr B2 the $K_{-1} > 0$ transitions peak locally at Sgr B2(N), near warm dust and likely IR excitation, whereas the lower critical density $K_{-1} = 0$ transitions arise from the more extended envelope (e.g., Churchwell et al. 1986; Kuan & Snyder 1996). The $K_{-1} = 0$ emission is strong toward the north and west edges of Sgr B2, near the CO "hole" seen in the molecular disk (Kuan & Snyder 1996; Minh et al. 1998), a hole that may have been created in a cloud-cloud collision (e.g., Hasegawa et al. 1994; Mehringer et al. 1995; Sato et al. 1998). (2) HNCO is distributed differently from $C^{18}O$ and is significantly enhanced in another Galactic center cloud known to have strong shocks, GMC G+1.6−0.025 (Mauersberger & Bronfman 1998; Hüttemeister et al. 1998). (3) A recent study of dense cores in the Galactic disk finds a tight correlation between HNCO ($K_{-1} = 0$) and SiO, a well-established shock tracer suggesting the same production mechanism (Zinchenko et al. 2000).

Toward the northern bar end in IC 342 (GMC D′), X(HNCO) can be well above 10^{-9} over ∼100 pc scales. It seems unlikely that gas-phase chemistry can dominate in this region. Localized shocks/mantle evaporation due to star formation such as in Sgr B2 or the Orion hot core cannot provide the observed enhancement unless star formation is extreme and widespread here, which it is not. The PCA finds that HNCO has a morphology most similar to that of CH_3OH, which is expected to trace shocks. These extragalactic observations appear to suggest that HNCO is being liberated from grain mantles due to the action of large-scale shocks.

If the shock interpretation for the 3 mm HNCO emission is correct, it is somewhat surprising that the line width of HNCO seen toward GMC D′ is quite narrow. However, every other line peaking at GMC D′ is broadened by unresolved hyperfine structure except HNC (1–0), so HNCO's line width may appear "artificially" narrow. The narrow line width may be evidence that the shocks are not strong. Strong shocks ($v \sim 100$ km s^{-1}) are expected to destroy the molecules as they are released from the grains, and there are some suggestions of this in the Galaxy (Zinchenko et al. 2000). Large-scale shocks due to cloud-cloud collisions at orbital resonances appear optimal in this respect, because they are probably mild, correlated with magnetic fields, and operate coherently over many tens of parsecs.

5.5. *An Extragalactic Map of the* HCN/HNC *Ratio*

The HCN/HNC abundance ratio is also an astrochemical enigma. In thermodynamic equilibrium, HCN is highly favored over the rare HNC. However, in cold dark clouds in the Galaxy, HNC is observed to be of similar abundance to HCN, and up to a factor of 3 more abundant (Hirota et al. 1998). In hotter regions such as the Orion hot core, HNC is still present but HCN dominates, with $[\mathrm{HCN}]/[\mathrm{HNC}] \sim 100$ (e.g., Goldsmith et al. 1981; Churchwell et al. 1984; Schilke et al. 1992; Turner et al. 1997). This has been interpreted as a transition from a chemical pathway that forms HNC and HCN at roughly equal abundances at low temperatures to neutral-neutral reaction paths with a small activation energy ($E_a \sim 200$ K) that takes over, creating HCN at the expense of HNC, at warm temperatures (Schilke et al. 1992; Hirota et al. 1998). Hence, a low HCN/HNC ratio has been considered a tracer of cool, quiescent gas.

From a theoretical perspective, the HCN/HNC abundance ratio is much cloudier. Standard model chemistry predicts a ratio of unity over a wide range of conditions (e.g., Lee et al. 1996), but with considerable uncertainties in the reactions. Recent models have suggested that the reaction $HCNH^+ + e^- \rightarrow HCN/HNC + H$ either slightly favors HNC over HCN (Shiba et al. 1998) or is equally probable (Talbi & Herbst 1998). If so, in cold dark clouds where cosmic-ray–driven ion-molecule chemistry dominates, it may be possible to explain the low observed HCN/HNC ratios. However, the dependence of the ratio on temperature is still largely unexplained. Given the observational evidence that the HCN/HNC ratio increases with temperature, neutral-neutral reactions with small activation energies that would preferentially destroy HNC in high temperature gas have been sought. Two commonly suggested reactions include

$$\mathrm{HNC} + \mathrm{H} \rightarrow \mathrm{HCN} + \mathrm{H}, \tag{12}$$

$$\mathrm{HNC} + \mathrm{O} \rightarrow \mathrm{NH} + \mathrm{CO} \tag{13}$$

(e.g., Schilke et al. 1992). The first reaction is especially promising because it converts HNC directly into HCN, effecting the HCN/HNC ratio sensitively. However, theoretical calculations suggest that both reactions have activation energies too large to contribute at gas temperatures less than several hundred kelvins (Talbi et al. 1996). Other reactions such as

$$\mathrm{N} + \mathrm{CH_2} \rightarrow \mathrm{HCN} + \mathrm{H} \tag{14}$$

have been suggested (e.g., Goldsmith et al. 1981; Turner et al. 1997), but are calculated to be exothermic enough to undergo isomerization upon relaxation, and therefore actually end up making equal amounts of HNC and HCN (Herbst et al. 2000).

Observations of HCN and HNC in starburst and Seyfert galaxies often find HCN/HNC ∼ 1, typical of Galactic dark clouds (Hüttemeister et al. 1995b; Aalto et al. 2002). Moreover, no correlation is seen between high HCN/HNC ratios and any typical indicator of high gas temperature. It is not clear that these observations even support the notion that HCN/HNC is an indicator of temperature (e.g., Aalto et al. 2002). However, it is difficult to interpret single-dish ratios, given the large physical size they subtend on the galaxy. It is in this context that we investigate the high-resolution GMC-to-GMC changes in the HCN/HNC ratio in IC 342.

In Figure 8 and Table 8, we use our HNC data together with HCN data kindly provided by D. Downes (Downes et al. 1992) to present the first high-resolution HCN/HNC line ratio map in an external galaxy. The HCN/HNC line ratio is ∼1–2, and fairly constant over the nuclear region. GMC A has the highest ratio of 2. While GMC A appears somewhat hotter than the ambient gas in IC 342 (MT01), it is not the hottest GMC

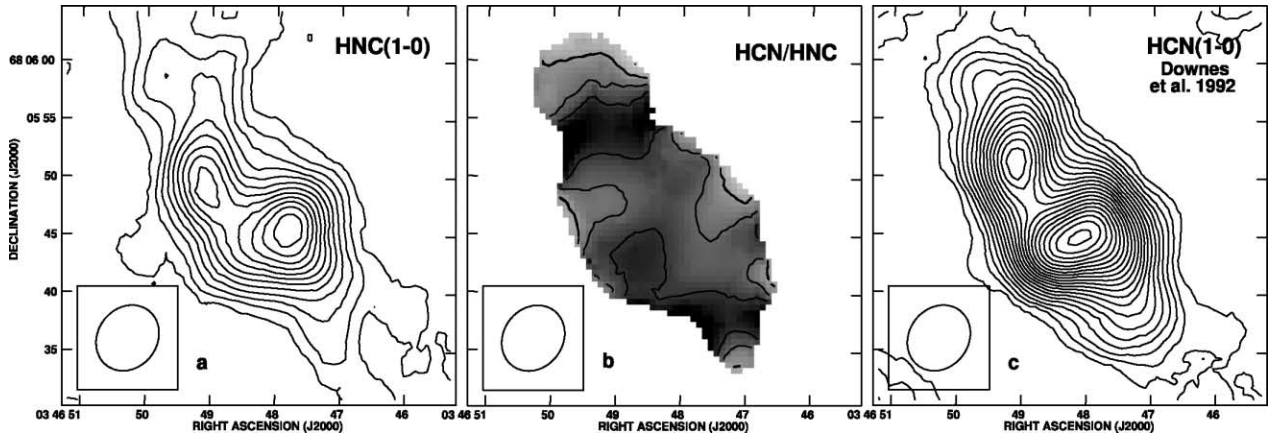

FIG. 8.—HCN (1–0)/HNC (1–0) line ratio. (*a*) HNC (1–0) integrated intensity map in contours of 2.5 K km s^{-1} for the beam size given in Table 1. (*b*) HCN (1–0)/HNC (1–0) line ratio map toward IC 342. Contours are 0.5, 1.0, 1.5, and 2.0, with the HCN/HNC = 1.0 contour in bold. (*c*) The HCN (1–0) integrated intensity map of Downes et al. (1992), convolved to the same resolution, plotted on the same scale and with the same contours.

(GMC B, $T_{ex} \sim 20$ K), nor is it near the present star formation and IR sources (GMCs B and C). In fact, starburst GMCs B and C are actually local minima of HCN/HNC. Finally, although the interpretation is limited somewhat by the smaller primary beam of the Plateau de Bure HCN (1–0) data, it does appear that there is a real trend for the HNC/HNC line ratio to decrease below unity as one goes to large distances from the center along the northern and southern spiral arms.

If we assume that HCN/HNC traces temperature and we use the Hirota et al. (1998) empirical Galactic dependence, then across the entire nuclear region this ratio would predict that T_k is approximately constant at 22–27 K. This is low compared to the observed dust temperature, 42 K, and gas kinetic temperatures of ~50 K in ammonia or the observed antenna temperature of the ^{12}CO (2–1) transition (Turner et al. 1993; Schinnerer et al. 2003). The explanation for the low HCN/HNC values could be that IC 342 has an abundant dense component that is significantly cooler and more uniform than the more diffuse component traced by CO. We consider this unlikely, since the CO, HNC, and HCN distributions are nearly coextensive. We consider more likely the possibility that HCN/HNC is simply not a function of temperature.

We have assumed that the HCN (1–0)/HNC (1–0) line ratio reflects the abundance ratio. This is only true if the line opacities are small. For $\tau > 1$, HCN (1−0)/HNC (1−0) ~ 1, independent of chemistry. Such an effect is most relevant where the line intensities are the highest, namely GMCs B and C. This is where the ratio approaches unity despite the proximity to H II regions. However single-dish observations of H^{13}CN (1–0) in IC 342 show that HCN (1−0)/H^{13}CN (1−0) ≃ 30 (Schulz et al. 2001), close to what is expected for the ^{12}C/^{13}C isotopic ratio in the nuclei of starburst galaxies (e.g., Henkel & Mauersberger 1993; Wilson & Rood 1994), indicating low opacities. Future high-resolution observations of H^{13}CN and HN^{13}C should provide information on this issue.

TABLE 8
SELECTED INTENSITY RATIOS

Location	HCN (1−0)[a] / HNC (1−0)	SO[b] / 23*C^{34}S
A	2.2 ± 0.4	<0.15
B	1.5 ± 0.3	<0.43
C	1.6 ± 0.3	<0.43
D	~0.99	<0.70
D′	~1.2	...
E	1.6 ± 0.3	0.72

NOTES.—The measurements of the HCN/HCN ratio are based on the resolution of HNC (1–0) given in Table 1. The uncertainties reflect the larger of the absolute calibration uncertainty or the map noise. Upper limits are 2 σ.

[a] HCN (1–0) is kindly provided by Downes et al. (1992).

[b] The SO/CS *abundance* ratio based on the most constraining of the SO upper limits.

5.6. *Quiescent Gas Tracer?* N_2H^+

It has been suggested that N_2H^+ is a robust tracer of the dense, quiescent component of molecular gas (e.g., Womack et al. 1992b). N_2H^+ abundances tend to be low in hot cores, outflows, and PDRs in the Galaxy. Hence, the extent and brightness of N_2H^+ in the nucleus of IC 342, with its active star formation, radiation, and shocks, is surprising. One might infer that dense gas is present in IC 342, but that this gas is largely sterile and quiescent with "dark cloud like" chemical conditions. In this picture, shocks, winds, and outflows associated with star formation are confined to small regions around each forming star, and the remaining dense gas is largely undisturbed. This would have interesting ramifications for the extremely luminous ($L_{IR} \sim 10^8\ L_\odot$) star-forming GMCs, B and C, which are both strong sources of N_2H^+ emission.

Alternatively, there could be differences in the formation or destruction rates of N_2H^+. N_2H^+ is formed almost exclusively from the reaction

$$N_2 + H_3^+ \rightarrow N_2H^+ + H_2 \qquad (15)$$

and is destroyed primarily by dissociative recombination with electrons in diffuse gas and by the ion-neutral reactions with CO and O in dark clouds. Therefore, N_2 is cycled through N_2H^+, and if the abundance of H_3^+ and electrons can be assessed, then N_2H^+ is a direct tracer of the (otherwise invisible) molecular nitrogen (e.g., Womack et al. 1992a; Turner 1995; Benson et al. 1998).

The H_3^+ abundance is formed from cosmic-ray ionization of H_2 and destroyed by reactions with e^-, CO, and O. In steady state,

$$X(H_3^+) = \frac{\zeta/n_{H_2}}{k_{H_3,O}X(O) + k_{H_3,CO}X(CO) + k_{H_3,e}X(e^-)}, \qquad (16)$$

where ζ is the cosmic-ray ionization rate and the rate coefficients k are taken from Benson et al. (1998) and Dalgarno & Lepp (1984), except for the dissociative recombination rate ($k_{H_3,e}$), which is taken from McCall et al. (2003). If we assume that N_2H^+ is formed by equation (15), then

$$\frac{X(N_2)}{X(N_2H^+)} = \frac{k_{N_2H,CO}X(CO) + k_{N_2H,e}X(e^-)}{k_{H_3,N_2}X(N_2)X(H_3^+)}, \quad (17)$$

or

$$\frac{X(N_2)}{X(N_2H^+)} = \left[k_{N_2H,CO}X(CO) + k_{N_2H,e}X(e^-)\right] \times \left[k_{H_3,O}X(O) + k_{H_3,CO}X(CO) + k_{H_3,e}X(e^-)\right] \times \left\{k_{H_3,N_2}X(N_2)[\zeta/n_{H_2}]\right\}^{-1}. \quad (18)$$

In this steady state chemical scheme, the abundance of N_2H^+ increases with (1) increasing ζ, (2) decreasing density, (3) decreasing electron fraction $X(e^-)$, or (4) increasing N_2, assuming that the CO and O abundances remain fairly constant across the nucleus. It seems unlikely that explanations 2 and 3 are dominant in the nucleus of IC 342. We know that the densities are high, at least a few $\times 10^4$ cm^{-3}, and that $X(e^-)$ could be as high as $\simeq 1.5 \times 10^{-5}$ based on the C^+ abundance determined by Crawford et al. (1985) and Eckart et al. (1990). The most likely possibility for the bright, extensive N_2H^+ emission is therefore either a high cosmic-ray ionization rate or enhanced N_2 abundance.

Figure 9 displays the $X(N_2)/X(N_2H^+)$ ratio as a function of electron fraction for different values of ζ/n_{H_2} (see eq. [17]). It has been assumed that $X(O) \simeq X(CO) = 10^{-4}$. The maximum N_2 abundance possible is one-half the total cosmic N abundance, or $X(N_2) \sim 4 \times 10^{-5}$ (e.g., Anders & Grevesse 1989). The brightness of the high-density tracers suggests that n_{H_2} is at least 10^4–$10^{4.5}$ cm^{-3}, implying that $\zeta_{IC\,342} > 10^{-17}$ s^{-1}, at least the Galactic disk value. If some N is not in N_2H^+ (and there is bright ammonia emission; Ho et al. 1990) or n_{H_2} is greater than 10^4 cm^{-3}, then ζ is constrained to be higher than the Galactic rate. For $X(e^-) \gtrsim 10^{-7}$, the cosmic-ray rate would have to be greater still. Therefore, to explain the bright and ubiquitous N_2H^+ emission, it is likely that $\zeta > 10^{-17}$ s^{-1} in the nucleus of IC 342.

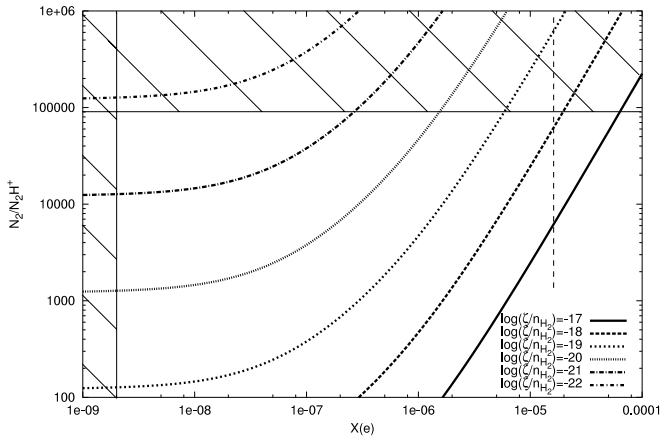

FIG. 9.—N_2/N_2H^+ abundance ratio as a function of various physical parameters, based on the basic, steady state chemical model described in § 5.5. The hashed-out regions of $X(e^-) < 2 \times 10^{-9}$ and $N_2/N_2H^+ > 9 \times 10^4$ are forbidden because it is assumed that the ISM is neutral [$X(e^-) > X(HCO^+) + X(N_2H^+)$] and that the maximum N_2 abundance is one-half of the cosmic N abundance, respectively. The observed $X(C^+)$ [$\simeq X(e^-)$] abundance is also marked (*thin dashed line*). However, this value likely applies to the diffuse molecular gas component, not the dense GMC component traced in N_2H^+. The thick contours mark the N_2/N_2H^+-$X(e^-)$ values for different values of the cosmic ionization rate per molecular gas density, $[\zeta/n_{H_2}]$. Assuming $n_{H_2} > 10^4$ cm^{-3}, expected for the excitation of bright N_2H^+, $\log(\zeta/n_{H_2}) \lesssim 10^{21}$ corresponds to a Galactic cosmic ionization rate. For such an ionization rate, $X(e^-) < 10^{-7}$ and $N_2 \gtrsim 1 \times 10^{-5}$. If $n_{H_2} \gtrsim 5 \times 10^{-4}$ cm^{-3} in the N_2H^+ emitting regions, then $\zeta_{IC\,342}$ must be larger than the Galactic disk value.

5.7. *The Warm and the Dense:* HC_3N

HC_3N has the highest upper energy state and one of the highest critical densities of our sample. The most striking feature of the HC_3N (10–9) intensity distribution is how closely it follows the 3 mm continuum emission. We consider two possibilities for the bright HC_3N emission in regions where the millimeter continuum is high: (1) enhanced HC_3N abundance toward star-forming GMCs B and C (and possibly E), or (2) that HC_3N is more highly excited by collisions with molecular hydrogen at the sites of the densest and warmest gas.

HC_3N formation is uncertain, but probably forms from the neutral-neutral reaction

$$C_2H_2 + CN \rightarrow HC_3N + H \quad (19)$$

and is destroyed by photodissociation and reactions with C^+ (e.g., Sims et al. 1993; Fukuzawa & Osamura 1997; Turner et al. 1998). Since the central-ring region has high abundances of C_2H, it is reasonable to expect that this region will also have high abundances of CN and C_2H_2, species that can maintain large abundances in PDRs. It is possible, therefore, that the high estimated HC_3N abundances follow from CN and C_2H_2 abundances here. The weakness of HC_3N toward GMC A would then be attributed to increased destruction rates due to photodissociation and large C^+ abundances and more diffuse gas working in tandem.

The second possibility for the HC_3N morphology is excitation. HC_3N is the molecule most sensitive to decreases in T_{ex} (decreases in density; Table 2). If there is an excitation gradient decreasing with distance from the starburst, the abundances derived outside the central starburst region would be artificially low. Given the sensitivity of the derived HC_3N abundance to excitation, we do not at this stage overinterpret possible changes in HC_3N chemistry and conclude that decreasing excitation away from the starbursts is the simplest explanation of the HC_3N morphology.

If excitation is the answer, then why is HC_3N not also bright at GMC A, since N_2H^+ and HNC (and HCN) are bright there, species with critical densities nearly as high or higher than HC_3N? GMC A is actually one of the warmer GMCs (in CO), so chemical changes may be favored. However, there is another possibility. Electrons could be responsible for some of the collisional excitation toward GMC A. In Table 2 the critical densities for electron collisions are compared with those for H_2 collisions. If $X(e^-) = X(C^+) \simeq 1.5 \times 10^{-5}$ in the center of IC 342 (Crawford et al. 1985; Eckart et al. 1990), then electrons are of equal or greater importance as a collision partner for N_2H^+, HCN, and HNC. For all other species, with the possible exception of $C^{34}S$ (2–1), collisions with electrons are not relevant. The C^+ abundance is almost certainly lower than the above values everywhere except GMC A and the central trough given that the C^+ value was made with a large beam and likely is dominated by the more diffuse molecular cloud component associated with the PDRs. Evidently, in the regions with abundant

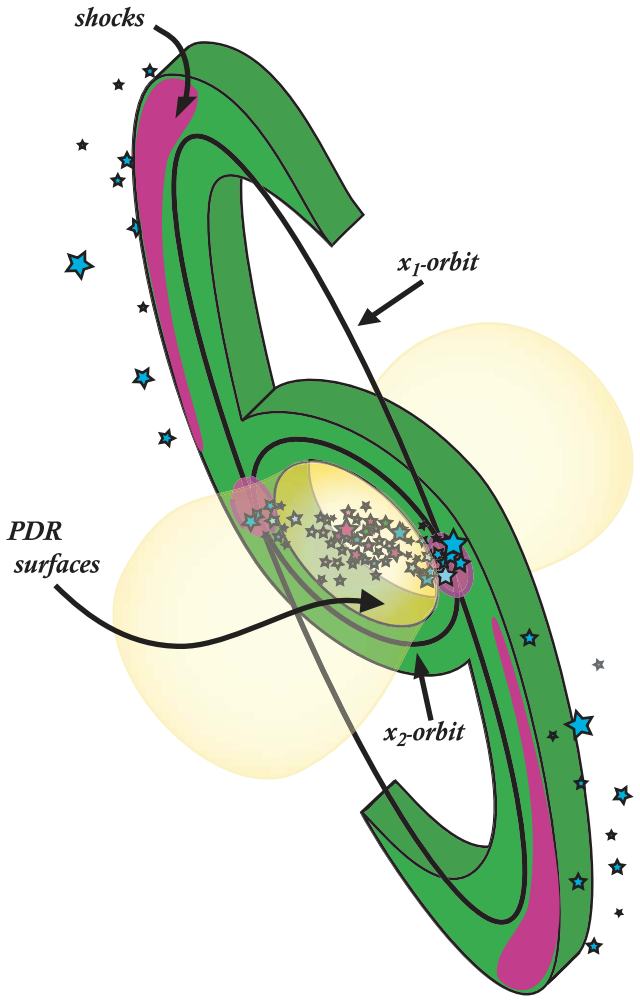

FIG. 10.—Schematic of the chemical and physical structure of the nucleus of IC 342.

C^+, HNC and HCN can be efficiently excited by electrons (Dickinson et al. 1977; Turner et al. 1997). This may have important consequences for densities derived from HCN in starburst galaxies dominated by PDR regions.

5.8. *The Overall Chemistry of IC 342*

When we consider all the observed molecular lines together, a consistent picture of the structure of the ISM in IC 342 begins to emerge, which is summarized in the cartoon of Figure 10. Gas response to a barred potential has set up the molecular minispiral within the nucleus of IC 342. Energy dissipation from cloud collisions and star formation within the molecular arms, and angular momentum transfer from tidal torquing, results in a gradual inward drift of molecular gas along the arms. Molecular gas piles up at the intersections of the arms and the central ring, where it triggers star formation at the rate of $\sim 0.1\ M_\odot\ \mathrm{yr}^{-1}$. In turn, the bar sets up density gradients both azimuthally along the molecular arms and radially. The molecular gas densities tend to be higher on the leading (counterclockwise) edges of the molecular arms, becoming more diffuse behind the arms (Wright et al. 1993; MT01). Densities also tend to be higher as the gas approaches the nucleus, peaking near the x_1-x_2 intersection. Compare the morphology of ^{12}CO (1–0), $C^{18}O$ (1–0), HNC, and HC_3N in Figure 2 to see the density progression from diffuse to dense gas.

The sphere of influence of the nuclear bar extends not just to the physical conditions of the gas (density, temperature) but also to the chemistry. CH_3OH and HNCO delineate the locations of shocks associated with cloud-cloud collisions within spiral arms, following the theoretical expectations of the locations of shocks in a barred potential (e.g., Athanassoula 1992). These molecules indicate that grain mantle liberation is important toward GMC D′ and possibly GMC C along the northern arm. The lack of the expected symmetry between the northern and southern arms appears to be due to a lower column density of dense gas toward the southwestern arm (Fig. 6*a*). Outside of GMC A it may be that grain liberation influences the abundances of most of the observed species either directly (CH_3OH and HNCO) or indirectly due to injection of "invisible" N_2 and C_2H_2 (N_2H^+ and HC_3N). It is tempting to speculate that the prevalence of molecular arm shocks explain why star formation is not pronounced along the spiral arms, but "waits" till the gas arrives in the central ring.

From C_2H and $C^{34}S$, we learn that the faces of the molecular ring surrounding the central star forming complex are bright PDRs. The limited spatial extent of C_2H argues that the C^+ abundance is strongly enhanced in the central ring; the primary ionization sources are not distributed uniformly across the nucleus, nor does the ionization appear to penetrate deeply into most of the GMCs. This rules out more penetrative mechanisms such as cosmic-ray ionization (primary or secondary) or hard X-rays as the main source of enhanced C^+ ionization in IC 342. Photoionization from stars is likely to produce enhanced C^+ given the interstellar radiation field is $\sim$320 times stronger than Galactic value (Israel & Baas 2003). This provides further support for previous studies that suggested that PDRs play an important role in the physical conditions of the central ring of IC 342 (Turner et al. 1993; MTH00; Schulz et al. 2001). Synchrotron emission (Fig. 3*a*; Turner & Ho 1983) indicates that supernovae have taken place in the nucleus, and one might expect the cosmic-ray ionization rate to be somewhat elevated there. The bright N_2H^+ emission alludes to such a possibility. Since the PCA analysis demonstrates that N_2H^+ and $C^{18}O$ have similar morphologies, whatever process elevates the N_2H^+ abundance operates fairly uniformly across the entire region, as would be expected for cosmic-ray ionization.

From the morphology of C_2H, the most likely source of ionizing radiation for the PDRs (see especially the inner face of GMC C) is the more mature ($\sim$60 Myr old) central nuclear cluster, and not the youngest ($\sim$a few Myr) star-forming regions seen in radio and millimeter continuum toward GMCs B and C. Evidently, the young stars in these large H II regions have yet to break out of their natal cocoons and influence the large-scale chemistry of the nucleus. The *HST* composite image, the preferentially blueshifted C_2H and $C^{34}S$ line profiles, and the weak C_2H extension perpendicular to the major axis imply that the central star formation event is just beginning to break out along the galactic minor axis.

GMC A appears to be the molecular cloud most strongly penetrated by UV photons. GMC A is also the only GMC in the central ring that is not a site of strong current star formation. These results suggest that for some reason GMC A is on average more diffuse than the other two GMCs, and therefore more susceptible to UV radiation. The reason for this is unclear, but may be related to its location in the nucleus. Close to the dynamical center of the galaxy and at a position where it likely has just "whipped" around from the x_1 orbital onto the x_2 orbital, tidal and shearing forces may be shredding cloud A apart (note the broad $C^{34}S$ line profile). In this condition, cloud

A is probably not inclined to collapse and form stars (until it collides with GMC B+E?).

It has been established that the chemistry of the two nearest prototypical starburst galaxies, M82 and NGC 253, have different chemical makeups (e.g., Mauersberger & Henkel 1991a; Henkel et al. 1991; Mauersberger & Henkel 1993). M82 is bright in HCN, HNC, C_2H, CN, HCO^+, and HCO, but notoriously weak in lines of SiO, CH_3OH, CH_3CN, HNCO, and SO, as compared to NGC 253 (Mauersberger & Henkel 1993; Takano et al. 1995). In IC 342, we see for the first time regions with M82-like chemistry (GMC A) and regions of NGC 253–like chemistry (GMC D′) in the same nucleus. Regions where grain disruption due to shocks occurs are likely to manifest chemistries similar to NGC 253, whereas sites of PDRs manifest M82-like chemistries. It is therefore tempting to conclude that the ISM in M82 is dominated by GMC A–type molecular gas (PDRs) and is deficient in GMC D–type molecular gas (shock/grain process species) due to absence of strong nucleus-wide shocks compared to the barred galaxy NGC 253. This lends support to similar conclusions reached by García-Burillo et al. (2000) and García-Burillo et al. (2002) for NGC 253 and M82. It also illustrates that CH_3OH and HNCO hold the potential of being a much more useful shock tracers in external galaxies than the well-established tracer SiO, since the 3 mm transitions of these two molecules are much brighter than SiO (Nguyen-Q-Rieu et al. 1991; Sage & Ziurys 1995; Hüttemeister et al. 1997). In IC 342 PDRs still remain largely confined to the central ring, but in M82 they are clearly much more pervasive.

Finally, an intriguing result of this data set is the apparent discovery of an isolated nitrogen-rich GMC. Its location between GMCs A and B suggests two possibilities. First, it is seen at the location where gas going down the northern arm collides with the southern arm. This may then represent a location of N_2 injection (from grain disruption), which would explain the increased N_2H^+ abundance and HNCO, but not necessarily the HC_3N abundance (unless C_2H_2 is also injected). A second possibility is that this region is enriched in ejecta from young, massive stars, perhaps Wolf-Rayet stars. There is a young, massive cluster seen in the near-infrared (NIR) near this location (see Fig. 3 of Schinnerer et al. 2003). There is evidence that massive star enrichment of ^{18}O has taken place in the central trough vicinity (MT01). But why is the nitrogen enrichment seen in this one location when there are several other NIR bright clusters, including the much larger central cluster, which are not known to be enriched? Similar studies of other galaxies may shed light on this question.

6. CONCLUSIONS

We have detected emission from a number of molecules in the central region of IC 342 at resolution of 5″ using OVRO. Significant differences are seen in the spatial distributions of these molecules, and we have analyzed the causes of these differences. Our main results include the following:

1. A principal-component analysis of the maps of the seven detected molecules, ^{12}CO (1–0), $C^{18}O$, HCN (1–0), and 3 mm continuum reveals that the maps all have some degree of correlation and that the dominant common factor (PC1 axis) is the density-weighted mean column density. Molecules with the largest projections on PC1 are N_2H^+, $C^{18}O$, and HNC. These molecules, and primarily N_2H^+, give the best overall representation of the total molecular gas distribution.

2. Differences in excitation and critical density are not the dominant influences shaping the spatial differences among the different molecules in IC 342, since the excitation energies of the transitions are similar and cloud densities are high enough that most molecules are collisionally excited.

3. The spatial differences among the molecular line emission are not driven by variations in chemical timescale: all clouds in this region are likely to have early-time chemistry due to the short orbital timescales of the nucleus.

4. The second principal component axis, PC2, splits into two anticorrelated groups of molecules: molecules that peak within the central 75 pc near GMC A and the nuclear star cluster, and those that peak up along the prominent northeastern arm, located 100–200 pc away from the nucleus.

5. The GMC A peakers, C_2H and $C^{34}S$, are enhanced in the center of IC 342 by high radiation fields. GMC A is a PDR cloud. The fact that these molecules tend to favor the parts of the clouds toward the center of IC 342 rather than toward the slightly off-center $L_{IR} \sim 10^8\ L_\odot$ radio/IR source suggests that the source of the radiation field affecting the chemistry of GMC A is the ~60 Myr central star cluster and not the actively star-forming radio/IR sources.

6. Molecules that peak along the northeast arm of the molecular minispiral are HNCO and CH_3OH. Large scale shocks due to the changes in gas velocity at the arms of the nuclear minispiral are probably the cause of enhanced HNCO and CH_3OH there.

7. HCN and HNC are the best tracers of the dense gas and HC_3N of warm, dense gas. Their correlation with the 3 mm continuum is excellent. The HCN/HNC ratio is 1–2 across the nuclear region and appears to be unrelated to kinetic temperature.

8. The brightness and extent of emission from N_2H^+ suggests that the cosmic-ray ionization rate is higher than $\zeta > 10^{-17}\ s^{-1}$ in the nucleus of IC 342.

We appreciate the support and assistance of the faculty, staff, and postdocs at OVRO during the observations. We are grateful to D. Downes for kindly providing us access to the HCN (1–0) data. We thank M. Jura and L. E. Snyder for reading drafts of the paper, and E. C. Sutton, M. Morris, and R. Hurt for helpful discussions. An anonymous referee is also thanked for providing a detailed, helpful, and prompt report. D. S. M. acknowledges support from the Laboratory for Astronomical Imaging at the University of Illinois through NSF grant AST 02-28953. This work is also supported by NSF grants AST 00-71276 and AST 03-079950 to J. L. T. The Owens Valley Millimeter Interferometer is operated by Caltech with support from the NSF under grant AST 99-81546.

REFERENCES

Aalto, S., Polatidis, A. G., Hüttemeister, S., & Curran, S. J. 2002, A&A, 381, 783
Anders, E., & Grevesse, N. 1989, Geochim. Cosmochim. Acta, 53, 197
Athanassoula, E. 1992, MNRAS, 259, 328
Bachiller, R., & Perez Gutierrez, M. 1997, ApJ, 487, L93
Becklin, E. E., Gatley, I., Mathews, K., Neugebauer, G., Sellgren, K., Werner, M. K., & Wynn-Williams, C. G. 1980, ApJ, 236, 441
Benson, P. J., Caselli, P., & Myers, P. C. 1998, ApJ, 506, 743
Bergin, E. A., Ciardi, D. R., Lada, C. J., Alves, J., & Lada, E. A. 2001, ApJ, 557, 209

Bergin, E. A., Goldsmith, P. F., Snell, R. L., & Langer, W. D. 1997, ApJ, 482, 285
Bergin, E. A., Neufeld, D. A., & Melnick, G. J. 1998, ApJ, 499, 777
Bergin, E. A., et al. 2000, ApJ, 539, L129
Blake, G. A., Sutton, E. C., Masson, C. R., & Phillips, T. G. 1987, ApJ, 315, 621
Blake, G. A., et al. 1996, ApJ, 472, L49
Böker, T., Förster-Schreiber, N. M., & Genzel, R. 1997, AJ, 114, 1883
Brouillet, N., & Schilke, P. 1993, A&A, 277, 381
Chin, Y.-N., Henkel, C., Whiteoak, J. B., Langer, N., & Churchwell, E. B. 1996, A&A, 305, 960
Chung, H. S., Osamu, K., & Masaki, M. 1991, J. Korean Astron. Soc., 24, 217
Churchwell, E., Nash, A. G., & Walmsley, C. M. 1984, ApJ, 287, 681
Churchwell, E., Wood, D., Myers, P. C., & Myers, R. V. 1986, ApJ, 305, 405
Crawford, M. K., Genzel, R., Townes, C. H., & Watson, D. M. 1985, ApJ, 291, 755
Dahmen, G., Hüttemeister, S., Wilson, T. L., & Mauersberger, R. 1998, A&A, 331, 959
Dalgarno, A., & Lepp, S. 1984, ApJ, 287, L47
Demyk, K., Dartois, E., d'Hendecourt, L., Jourdain de Muizon, M., Heras, A. M., & Breitfellner, M. 1998, A&A, 339, 553
de Vicente, P., Martín-Pintado, J., Neri, R., & Colom, P. 2000, A&A, 361, 1058
Dickinson, A. S., Phillips, T. G., Goldsmith, P. F., Percival, I. C., & Richards, D. 1977, A&A, 54, 645
Di Francesco, J., Hogerheijde, M. R., Welch, W. J., & Bergin, E. A. 2002, AJ, 124, 2749
Downes, D., Radford, S. J. E., Giulloteau, S., Guelin, M., Greve, A., & Morris, D. 1992, A&A, 262, 424
Drdla, K., Knapp, G. R., & van Dishoeck, E. F. 1989, ApJ, 345, 815
Eckart, A., Downes, D., Genzel, R., Harris, A. I., Jaffe, D. T., & Wild, W. 1990, ApJ, 348, 434
Everitt, B. S., & Dunn, G. 2001, Applied Multivariate Data Analysis (London: Oxford Univ. Press), 48
Frerking, M. A., Langer, W. D., & Wilson, R. W. 1982, ApJ, 262, 590
Friberg, P., Hjalmarson, A., Madden, S. C., & Irvine, W. M. 1988, A&A, 195, 281
Fuente, A., Martín-Pintado, J., Cernicharo, J., & Bachiller, R. 1993, A&A, 276, 473
Fukuzawa, K., & Osamura, Y. 1997, ApJ, 489, 113
Gao, Y., & Solomon, P. M. 2004, ApJ, 606, 271
García-Burillo, S., Martín-Pintado, J., Fuente, A., & Neri, R. 2000, A&A, 355, 499
———. 2001, ApJ, 563, L27
García-Burillo, S., Martín-Pintado, J., Fuente, A., Usero, A., & Neri, R. 2002, ApJ, 575, L55
Goldsmith, P. F., Langer, W. D., Ellder, J., Kollberg, E., & Irvine, W. 1981, ApJ, 249, 524
Goldsmith, P. F., et al. 2000, ApJ, 539, L123
Gottlieb, C. A., Gottlieb, E. W., Litvak, M. M., Ball, J. A., & Penfield, H. 1978, ApJ, 219, 77
Graedel, T. E., Langer, W. D., & Frerking, M. A. 1982, ApJS, 48, 321
Green, S. 1975, ApJ, 201, 366
———. 1986, NASA Technical Memo 87791 (Washington, DC: NASA)
———. 1994, ApJ, 434, 188
Green, S., & Chapman, S. 1978, ApJS, 37, 169
Green, S., & Thaddeus, P. 1974, ApJ, 191, 653
Grim R. J. A., & Greenberg, J. M. 1987, ApJ, 321, L91
Harris, A. I., Stutzki, J., Graf, U. U., Russell, A. P. G., Genzel, R., & Hills, R. E. 1991, ApJ, 382, L75
Hasegawa, T. I., & Herbst, E. 1993, MNRAS, 263, 589
Hasegawa, T. I., Sato, F., Whiteoak, J. B., & Miyawaki, R. 1994, ApJ, 429, L77
Heikkilä, A., Johansson, L. E. B., & Olofsson, H. 1999, A&A, 344, 817
Heithausen, A., Corneliussen, U., & Grossmann, V. 1995, A&A, 301, 941
Helfer, T. T., & Blitz, L. 1993, ApJ, 419, 86
———. 1997, ApJ, 478, 162
Henkel, C., Baan, W. A., & Mauersberger, R. 1991, A&A Rev., 3, 47
Henkel, C., Jacq, T., Mauersberger, R., Menten, K. M., & Steppe, H. 1987, A&A, 188, L1
Henkel, C., & Mauersberger, R. 1993, A&A, 274, 730
Henkel, C., Schilke, P., & Mauersberger, R. 1988, A&A, 201, L23
Herbst, E., & Klemperer, W. 1973, ApJ, 185, 505
Herbst, E., Terzieva, R., & Talbi, D. 2000, MNRAS, 311, 869
Hirota, T., Yamamoto, S., Mikami, H., & Ohishi, M. 1998, ApJ, 503, 717
Ho, P. T. P., Martin, R. N., & Ruf, K. 1982, A&A, 113, 155
Ho, P. T. P., Martin, R. N., Turner, J. L., & Jackson, J. M. 1990, ApJ, 355, L19
Ho, P. T. P., Turner, J. L., & Martin, R. N. 1987, ApJ, 322, L67
Hudson, R. L., & Moore, M. H. 2000, A&A, 357, 787
Huggins, P. J., Carlson, W. J., & Kinney, A. L. 1984, A&A, 133, 347
Hüttemeister, S., Dahmen, G., Mauersberger, R., Henkel, C., Wilson, T. L., & Martín-Pintado, J. 1998, A&A, 334, 646
Hüttemeister, S., Henkel, C., Mauersberger, R., Brouillet, N., Wikland, T., & Millar, T. J. 1995a, A&A, 295, 571
Hüttemeister, S., Mauersberger, R., & Henkel, C. 1997, A&A, 326, 59
Hüttemeister, S., Wilson, T. L., Mauersberger, R., Lemme, C., Dahmen, G., & Henkel, C. 1995b, A&A, 294, 667
Iglesias, E. 1977, ApJ, 218, 697
Ishizuki, S., Kawabe, R., Ishiguro, M., Okumura, S. K., Morita, K.-I., Chikada, Y., & Kasuga, T. 1990, Nature, 344, 224
Israel, F. P., & Baas, F. 2003, A&A, 404, 495
Kalenskii, S. V., Dzura, A. M., Booth, R. S., Winnberg, A., & Alakoz, A. V. 1997, A&A, 321, 311
Kalenskii, S. V., & Sobolev, A. M. 1994, Astron. Lett., 20, 91
Karachentsev, I. D., Sharina, M. E., Dolphin, A. E., & Grebel, E. K. 2003, A&A, 408, 111
Keane, J. V., Tielens, A. G. G. M., Boogert, A. C. A., Schutte, W. A., & Whittet, D. C. B. 2001, A&A, 376, 254
Krzanowski, W. J. 1988, Principles of Multivariate Analysis (Oxford: Clarendon)
Kuan, Y., & Snyder, L. E. 1996, ApJ, 470, 981
Lapinov, A. V., Schilke, P., Juvela, M., & Zinchenko, I. I. 1998, A&A, 336, 1007
Lee, H.-H., Bettens, R. P. A., & Herbst, E. 1996, A&AS, 119, 111
Lepp, S., Dalgarno, A., van Dishoeck, E. F., & Black, J. H. 1988, ApJ, 329, 418
Levine, D., Turner, J. L., & Hurt, R. L. 1994, in IAU Colloq. 140, Astronomy with Millimeter and Submillimeter Wave Interferometry, ed. M. Ishiguro (ASP Conf. Ser. 59; San Francisco: ASP), 339
Lo, K. Y., et al. 1984, ApJ, 282, L59
Lucas, R., & Liszt, H. S. 2000, A&A, 358, 1069
———. 2001, A&A, 370, 576
———. 2002, A&A, 384, 1054
Martín, S., Martín-Pintado, J., Mauersberger, R., Henkel, C., & García-Burillo, S. 2004, ApJ, submitted
Martín, S., Mauersberger, R., Martín-Pintado, J., García-Burillo, S., & Henkel, C. 2003, A&A, 411, L465
Mauersberger, R., & Bronfman, L. 1998, Rev. Mod. Astron., 11, 209
Mauersberger, R., & Henkel, C. 1989, A&A, 223, 79
———. 1991a, A&A, 247, 307
———. 1991b, A&A, 245, 457
———. 1993, Rev. Mod. Astron., 6, 69
Mauersberger, R., Henkel, C., & Chin, Y.-N. 1995, A&A, 294, 23
Mauersberger, R., Henkel, C., Walmsley, C. M., Sage, L. J., & Wiklind, T. 1991, A&A, 247, 307
Mauersberger, R., Henkel, C., Weiß, A., Peck, A. B., & Hagiwara, Y. 2003, A&A, 403, 561
Mauersberger, R., Henkel, C., Wilson, T. L., & Harju, J. 1989, A&A, 226, L5
McCall, B. J., et al. 2003, Nature, 422, 500
Mehringer, D. M., De Pree, C. G., Gaume, R. A., Goss, W. M., & Claussen, M. J. 1995, ApJ, 442, L29
Meier, D. S., & Turner, J. L. 2001, ApJ, 551, 687 (MT01)
———. 2004, AJ, 127, 2069
Meier, D. S., Turner, J. L., & Hurt, R. L. 2000, ApJ, 531, 200 (MTH00)
Menten, K. M., Walmsley, C. M., Henkel, C., Wilson, T. L., Snyder, L. E., Hollis, J. M., & Lovas, F. J. 1986, A&A, 169, 271
Millar, T. J., Herbst, E., & Charnley, S. B. 1991, ApJ, 369, 147
Millar, T. J., & Nejad, L. A. M. 1985, MNRAS, 217, 507
Minh, Y. C., Haikala, L., Hjalmarson, A., & Irvine, W. M. 1998, ApJ, 498, 261
Minier, V., & Booth, R. S. 2002, A&A, 387, 179
Morata, O., Estalella, R., Lopez, R., & Planesas, P. 1997, MNRAS, 292, 120
Morris, M., & Serabyn, E. 1996, ARA&A, 34, 645
Morris, M., Turner, B. E., Palmer, P., & Zuckerman, B. 1976, ApJ, 205, 82
Murtagh, F., & Heck, A. 1987, Multivariate Data Analysis (Dordrecht: Reidel)
Nguyen-Q-Rieu, Henkel, C., Jackson, J. M., & Mauersberger, R. 1991, A&A, 241, L33
Nguyen-Q-Rieu, Jackson, J. M., Henkel, C., Truong, B., & Mauersberger, R. 1992, ApJ, 399, 521
Nguyen-Q-Rieu, Nakai, N., & Jackson, J. M. 1989, A&A, 220, 57
Nilsson, A., Hjalmarson, Å., Bergman, P., & Millar, T. J. 2000, A&A, 358, 257
Novozamsky, J. H., Schutte, W. A., & Keane, J. V. 2001, A&A, 379, 588
Nummelin, A., Bergman, P., Hjalmarson, Å., Friberg, P., Irvine, W. M., Millar, T. J., Ohishi, M., & Saito, S. 2000, ApJS, 128, 213
Nyman, L.-A. 1984, A&A, 141, 323
Nyman, L.-A., & Millar, T. J. 1989, A&A, 222, 231
Padin, S., Scott, S. L., Woody, D. P., Scoville, N. Z., Seling, T. V., Finch, R. P., Ciovanine, C. J., & Lowrance, R. P. 1991, PASP, 103, 461
Petuchowski, S. J., & Bennett, C. L. 1992, ApJ, 391, 137
Pickett, H. M., Poynter, R. L., Cohen, E. A., Delitsky, M. L., Pearson, J. C., & Muller, H. S. P. 1998, J. Quant. Spectrosc. Radiat. Transfer, 60, 883
Pottage, J. T., Flower, D. R., & Davis, S. L. 2004, MNRAS, 352, 39

Prasad, S. S., & Huntress, W. T. 1980, ApJ, 239, 151
Rickard, L. J., & Harvey, P. M. 1984, AJ, 89, 1520
Rydbeck, O. E. H., Hjalmarson, A., Rydbeck, G., Ellder, J., Kollberg, E., & Irvine, W. M. 1980, ApJ, 235, L171
Sage, L. J., & Ziurys, L. M. 1995, ApJ, 447, 625
Saha, A., Claver, J., & Hoessel, J. G. 2002, AJ, 124, 839
Sandell, G., Knee, L. B. G., Aspin, C., Robson, I. E., & Russell, A. P. G. 1994, A&A, 285, L1
Sato, F., Hasegawa, T. I., Whiteoak, J. B., & Shimizu, W. 1998, in IAU Symp. 184, The Central Regions of the Galaxy and Galaxies, ed. Y. Sofue (Dordrecht: Kluwer), 181
Schilke, P., Walmsley, C. M., Pineau des Forêts, G., Roueff, E., Flower, D. R., & Guilloteau, S. 1992, A&A, 256, 595
Schinnerer, E., Böker, T., & Meier, D. S. 2003, ApJ, 591, L115
Schulz, A., Güsten, R., Köster, B., & Krause, D. 2001, A&A, 371, 25
Schutte, W. A., & Greenberg, J. M. 1997, A&A, 317, L43
Schutte, W. A., Tielens, A. G. G. M., & Sandford, S. A. 1991, ApJ, 382, 523
Scoville, N. Z., Carlstrom, J., Padin, S., Sargent, A., Scott, S., & Woody, D. 1994, in IAU Colloq. 140, Astronomy with Millimeter and Submillimeter Wave Interferometry, ed. M. Ishiguro (ASP Conf. Ser. 59; San Francisco: ASP), 10
Seaquist, E. R., Frayer, D. T., & Frail, D. A. 1997, ApJ, 487, L131
Shiba, Y., Hirano, T., Nagashima, U., & Ishii, K. 1998, J. Chem. Phys., 108, 698
Sims, I. R., Queffelec, J.-L., Travers, D., Rowe, B. R., Herbert, L. B., Karthauser, J., & Smith, I. W. M. 1993, Chem. Phys. Lett., 211, 461
Solomon, P. M., Downes, D., & Radford, S. J. E. 1992, ApJ, 387, L55
Sorai, K., Nakai, N., Kuno, N., & Nishiyama, K. 2002, PASJ, 54, 179
Sternberg, A., & Dalgarno, A. 1995, ApJS, 99, 565
Swade, D. A. 1989, ApJ, 345, 828
Takano, S., Nakai, N., & Kawaguchi, K. 1995, PASJ, 47, 801
Talbi, D., Ellinger, Y., & Herbst, E. 1996, A&A, 314, 688
Talbi, D., & Herbst, E. 1998, A&A, 333, 1007
Truong-Bach, Nguyen-Q-Rieu, Omont, A., Olofsson, H., & Johansson, L. E. B. 1987, A&A, 176, 285
Turner, B. E. 1989, ApJS, 70, 539
———. 1991, ApJS, 76, 617
———. 1995, ApJ, 444, 708
———. 1996, ApJ, 461, 246
———. 1998, ApJ, 501, 731
Turner, B. E., Herbst, E., & Terzieva, R. 2000, ApJS, 126, 427
Turner, B. E., Lee, H.-H., & Herbst, E. 1998, ApJS, 115, 91
Turner, B. E., Pirogov, L., & Minh, Y. C. 1997, ApJ, 483, 235
Turner, B. E., Terzieva, R., & Herbst, E. 1999, ApJ, 518, 699
Turner, J. L., & Ho, P. T. P. 1983, ApJ, 268, L79
Turner, J. L., & Hurt, R. L. 1992, ApJ, 384, 72
Turner, J. L., Hurt, R. L., & Hudson, D. Y. 1993, ApJ, 413, L19
Ungerechts, H., Bergin, E., Goldsmith, P. F., Irvine, W. M., Schloeb, F. P., & Snell, R. L. 1997, ApJ, 482, 245
Usero, A., García-Burillo, S., Fuente, A., Martín-Pintado, J., & Rodriguez-Fernandez, N. J. 2004, A&A, 419, 897
van Broekhuizen, F. A., Keane, J. V., & Schutte, W. A. 2004, A&A, 415, 425
vanden Bout, P. A., Loren, R. B., Snell, R. L., & Wootten, A. 1983, ApJ, 271, 161
van Dishoeck, E. F., & Blake, G. A. 1998, ARA&A, 36, 317
Wall, J. V., & Jenkins, C. R. 2003, Practical Statistics for Astronomers (Cambridge: Cambridge Univ. Press)
Wang, M., Henkel, C., Chin, Y.-N., Whiteoak, J. B., Hunt Cunningham, M., Mauersberger, R., & Muders, D. 2004, A&A, 422, 883
Wang, Y., Jaffe, D. T., Evans, N. J., Hayashi, M., Tatematsu, K., & Zhou, S. 1993, ApJ, 419, 707
Watt, G. D. 1983, MNRAS, 205, 321
Watt, G. D., White, G. J., Millar, T. J., & van Ardenne, A. 1988, A&A, 195, 257
Weiß, A., Neininger, N., Hüttemeister, S., & Klein, U. 2001, A&A, 365, 571
Wilson, T. L., & Rood, R. 1994, ARA&A, 32, 191
Wilson, T. L., Snyder, L. E., Comoretto, G., Jewell, P. R., & Henkel, C. 1996, A&A, 314, 909
Womack, M., Ziurys, L. M., & Wyckoff, S. 1992a, ApJ, 393, 188
———. 1992b, ApJ, 387, 417
Wootten, A., Bozyan, E. P., Garrett, D. B., Loren, R. B., & Snell, R. L. 1980, ApJ, 239, 844
Wootten, A., Evans, N. J., Snell, R., & vanden Bout, P. 1978, ApJ, 225, L143
Wright, M. C. H., Ishizuki, S., Turner, J. L., Ho, P. T. P., & Lo, K. Y. 1993, ApJ, 406, 470
Xie, S., Young, J., & Schloerb, F. P. 1994, ApJ, 421, 434
Young, J. S., & Scoville, N. Z. 1991, ARA&A, 29, 581
Zinchenko, I., Henkel, C., & Mao, R. Q. 2000, A&A, 361, 1079